

NUSP-2

02 – 08

KNMI-publicatie: 201

Sciamachy Data Assimilation 2

Final Report

J.F. Meirink

H.J. Eskes

M. van Weele

H.M. Kelder



This report describes a project carried out in the framework of the National User Support Programme 2001 – 2005 (NUSP-2) under responsibility of the Netherlands Agency for Aerospace Programmes (NIVR).

Sciamachy Data Assimilation 2

Final Report

J.F. Meirink, H.J. Eskes, M. van Weele, H.M. Kelder

Royal Netherlands Meteorological Institute (KNMI)

NUSP-2 report 02 – 08

NUSP-2 project 4.1/AP-14

KNMI-publicatie: 201

januari 2003

ISBN 90-369-2227-5



This report describes a project carried out in the framework of the National User Support Programme 2001 – 2005 (NUSP-2) under responsibility of the Netherlands Agency for Aerospace Programmes (NIVR).

Contents

Abstract	3
Executive summary	5
1 A parameterized Kalman filter assimilation approach for long-lived trace gases	7
1.1 Introduction	7
1.2 The assimilation scheme	8
1.2.1 Superobservations	9
1.2.2 Forecast covariance parameterization	9
1.2.3 Covariance advection and error growth	10
1.2.4 Covariance analysis	11
1.2.5 Parameter estimates	11
1.3 Conclusion	12
2 Data assimilation of GOME ozone column data	13
2.1 Introduction	13
2.2 Ozone modelling	14
2.2.1 Transport	14
2.2.2 Chemistry	14
2.3 Observations	15
2.4 Assimilation	15
2.5 Data sets produced	15

2.6	Activities	16
3	Ozone forecasts	17
3.1	Introduction	17
3.2	The model and assimilation approach	18
3.2.1	Data assimilation results	20
3.2.2	Operational ozone forecasts	20
3.3	Anomaly correlation and RMS error	20
3.4	Ozone forecast examples	24
3.4.1	The year 2000 ozone hole	24
3.4.2	Low ozone episode over northern Europe	26
3.5	Conclusions	26
4	Assimilation of methane satellite data in a tracer transport model	29
4.1	Introduction	29
4.2	Current status of knowledge on methane	31
4.2.1	Emissions	31
4.2.2	Model simulations	32
4.3	The TM3 model, version TMSCIA	33
4.3.1	Simulation for the present case	35
4.3.2	Methane single-tracer version	37
4.4	Assimilation	37
4.4.1	Generation of synthetic data	37
4.4.2	Results of the assimilation	40
4.5	Conclusions	41
	Outlook	44
	Acknowledgements	45
	References	46

Abstract

The launch of the ESA ENVISAT satellite in March 2002 and near-future missions such as NASA EOS-AURA will largely expand the monitoring of the atmospheric chemical composition from space. Since 1995, GOME on ESA ERS-2 has provided a wealth of information on ozone and reactive trace gases such as NO₂. The SCIAMACHY spectrometer on ENVISAT extends the capabilities of GOME, and important additional information on greenhouse gases (including methane) and carbon monoxide is obtained from the channels in the near infrared. Data assimilation will play a crucial role in the near future to make optimal use of the huge observational data sets provided by SCIAMACHY and the other new satellite instruments.

In this project, ongoing activities on the assimilation of GOME near-real-time ozone observations in a global tracer-transport model are described. Three-dimensional value-added ozone fields are generated based on the GOME ozone observations. In addition, 5-day ozone forecasts were produced daily during the project. The quality of the analyses and forecasts is thoroughly evaluated. The operational products are provided to the scientific community via the KNMI web site.

The methane modelling capability of the TM3 chemistry-transport model has been further improved (model version TMSCIA). A data assimilation scheme has been developed for a methane single-tracer version of TMSCIA. This assimilation model is suitable for high resolution analyses of methane data. Tests with simulated data show that the system works well and is ready for the assimilation of SCIAMACHY observations.

Executive summary

The theme of the BCRS project *Sciamachy Data Assimilation* (phase 2) is the assimilation of satellite measurements of ozone and methane into global atmospheric models. A major goal is to provide global fields of these trace gases, and to allow scientists to access these data via the internet.

The trace gas ozone has a major impact on all aspects of the atmosphere. First, it is a key species in atmospheric chemistry, impacting on the distributions of many other gases in the atmosphere. Second, the depletion of stratospheric ozone as a consequence of anthropogenic CFC emissions is a long-recognized problem, and is the subject of the Montreal protocol. Third, ozone contributes to the greenhouse effect – subject of the Kyoto protocol – and changes in ozone have an impact on the heating and dynamics of in particular the stratosphere.

Methane (CH_4) is the second most important anthropogenic greenhouse gas, after carbon dioxide (CO_2). Since pre-industrial times the observed (from ice cores) 150% increase in the globally averaged CH_4 abundance has caused about 20% of the radiative forcing by all greenhouse gases together (estimates from IPCC 2001). Unlike CO_2 , CH_4 is chemically active: it is removed through oxidation by the highly variable OH radical. The oxidation capacity of the atmosphere is, in turn, strongly influenced by the abundances of ozone and nitrogen dioxide.

In order to simulate global distributions of O_3 and CH_4 , atmospheric models need to incorporate their atmospheric transport, chemical reactions, and emissions (for CH_4). Data assimilation involves the combination of such models with available observations in order to benefit from both. The increasing availability of satellite data makes this technique more and more useful.

SCIAMACHY, a UV-VIS-near-IR spectrometer measuring reflected sunlight, was launched successfully on the 1st of March 2002 on the ESA platform ENVISAT. The instrument will measure the ozone and methane column distributions globally. For O_3 the observations are an extension of the GOME instrument. Improvements are the smaller ground pixels and the combination of limb and nadir observations. The latter feature will allow to better distinguish between stratospheric and tropospheric contributions to the total column.

SCIAMACHY will also deliver CH_4 column measurements, which are unique in their coverage and expected accuracy. Most present-day satellite measurements of CH_4 are limited to stratospheric profiles such as from the HALOE/CLAES instruments on board of the UARS platform launched in 1991. Satellite observations of column amounts of CH_4 are only available from the MOPITT and IMG instruments, based on different measurement techniques. One of the aims of the project is to assist in the intercomparison between MOPITT and SCIAMACHY, as part of the ENVISAT core validation activities (in particular, the COMETH project).

In the first part of this report the assimilation of GOME near-real-time ozone observations, and the operational production of 5-day ozone forecasts from the analyses are described. It is shown

that medium-range ozone forecasts can be performed with a quality similar to geopotential height anomaly forecasts. The main achievements of this part of the work are:

- The model TM3DAM, developed during the first phase of the Sciamachy Data Assimilation project, has been further improved, and has been ported to the new SUN supercomputer at the KNMI. The operational ozone analyses and forecasts are monitored on a daily basis. The data can be accessed via the KNMI web site (http://www.knmi.nl/gome_fd).
- The pre-processing, at the ECMWF, of the meteorological fields that drive the model has been updated. TM3DAM now uses improved mass fluxes derived directly from the spectral vorticity and divergence fields.
- Two papers have been written. The first is about the TM3DAM model and assimilation aspects; the second about the forecast performance.

In the second part an assimilation system for CH₄ columns is presented. Since SCIAMACHY observations are not yet available, the system is tested with synthetic data together with estimated observation errors. These tests indicate that the system works well and is ready for the assimilation of SCIAMACHY data. This part of the work is closely related to the BCRS project MEGGY, in which the potential to retrieve continental-scale relative emissions from SCIAMACHY CH₄ column observations was investigated. The main achievements are:

- Multi-year runs have been performed with the TM3 model (version TMSCIA, developed, as a part of MEGGY, in particular for the interpretation of SCIAMACHY observations) to test the modelling capabilities for methane.
- A single-tracer version of TMSCIA has been developed, which makes high-resolution ($2.5^\circ \times 2.5^\circ$) runs feasible.
- This tracer version has been coupled to the assimilation software that is also used in TM3DAM.

Chapter 1

A parameterized Kalman filter assimilation approach for long-lived trace gases

A data assimilation scheme is described to assimilate GOME and SCIAMACHY total column trace gas observations, in particular ozone and methane. The assimilation approach is based on the Kalman filter equations. The scheme provides detailed and realistic maps of the forecast error. The model error and correlations are described in terms of parameters, fixed by the observation minus forecast statistics. Despite this detailed forecast error modeling, the computationally expensive aspects of the Kalman filter are avoided and the analysis scheme is very efficient.

1.1 Introduction

Data assimilation is at the core of modern numerical weather forecasting. The model forecast is combined with various types of observations to construct a description of the atmosphere consistent with both sources of information. This analysis provides a global description of the state of the atmosphere and it is the basis for a reliable medium-range weather forecast. In the field of atmospheric chemistry the use of data assimilation is still new, although similar benefits can be expected. Existing satellite instruments such as the Total Ozone Mapping Spectrometer (TOMS), the Solar Backscatter UV (SBUV and SBUV-2), and the Global Ozone Monitoring Experiment (GOME) provide extensive data sets of ozone and other chemical species. In the near future, the Scanning Imaging Absorption Spectrometer for Atmospheric Cartography (SCIAMACHY) on board of ENVISAT will deliver measurements of various trace gases, including ozone and methane. With data assimilation these observational data sets can be combined with knowledge of the dynamics and chemistry of the atmosphere to provide global 3D maps of the

chemical composition consistent with the available observational data.

Because of the widely available satellite ozone data sets a majority of the assimilation studies so far have focused on this compound. An overview of work in this direction, performed at KNMI with BCRS support, is given in chapter 2. This work has led to the development of an efficient data-assimilation scheme, using a parameterized Kalman filter approach. This scheme is not only suitable for the assimilation of ozone, but also of other trace gases.

Since the assimilation scheme is the central element of this report (it is used for ozone as well as methane assimilation) this first chapter gives a general description of the assimilation scheme. For additional information we refer to Eskes et al. (2001) and Eskes et al. (2002b).

1.2 The assimilation scheme

The assimilation scheme is based on the Kalman filter equations. However, it avoids the time and memory consuming steps in the Kalman filter (the forecast covariance advection and analysis) by parameterizing the horizontal correlations between forecast errors. As a result, the scheme is fast, and thus of great practical use, and it produces realistic error bars (time and space dependent forecast error fields) for the assimilated fields. Several aspects of the error modelling approach have been discussed before in Eskes et al. (1999) and Jeuken et al. (1999).

The Kalman equations consist of a forecast and analysis equation for the 3D tracer field \vec{x} , and similar forecast and analysis equations for the forecast error covariance matrix \mathbf{P} . The forecast equation for the field consists of applying the model \mathbf{M} to the tracer field \vec{x}_t^f at time t . The analysis for the field is given by,

$$\vec{x}_t^a = \vec{x}_t^f + \mathbf{P}\mathbf{H}^T (\mathbf{H}\mathbf{P}\mathbf{H}^T + \mathbf{R})^{-1} (\vec{y}^o - \mathbf{H}\vec{x}_t^f). \quad (1.1)$$

The forecast field \vec{x}^f is replaced by the analysis \vec{x}^a by incorporating the information provided by the observations \vec{y}^o . The matrix \mathbf{H} , the observation operator, computes an estimate of the observation (the total column of the tracer at a particular latitude and longitude) based on the 3D model field. \mathbf{R} is the combined observation and representativeness error covariance. Solving this equation with fixed covariance matrices is called “statistical interpolation” or “optimal interpolation”.

It is convenient to define the model tracer fields as $x_{i,l}$ = (partial) tracer column (in DU) in the (lat,lon) grid cell with index i and in the layer with index l . In this case the observation operator H becomes dimensionless and is independent of the layer index l : the total ozone column is a simple sum over the layer columns.

1.2.1 Superobservations

To reduce the computational effort, the assimilation is performed with "superobservations". This means that all satellite ground pixels with central coordinates in model grid cell i are treated as one observation. First, the model ozone field is interpolated to the position of each of the pixels, and the ozone column innovation vector $(y - Hx)$ is computed. Subsequently the average innovation in grid cell i is computed as $(y - Hx)^{superobs} = 1/M_i \sum (y - Hx)$, where M_i is the number of pixels in grid cell i . If c represents an average error correlation between the observations in cell i , then the error of the superobservation can be approximately related to the error of the individual satellite observations (Jeuken et al. 1999) by,

$$\sigma_i^{superobs} = \sigma^{obs} \sqrt{\frac{1-c}{M_i} + c}. \quad (1.2)$$

In the rest of this paper the innovation $(y - Hx)$ will refer to these superobservation innovations.

1.2.2 Forecast covariance parameterization

The forecast covariance matrix consists of N times N statistical parameters. These parameters are in principle determined by investigating the forecast error correlations over large statistical samples. In practice only a few parameters can be determined in this way. In particular, for the assimilation of trace-gas columns there is no direct information on how the forecast error behaves as a function of the vertical layer index l .

The covariance matrix \mathbf{P} is modelled by the following expression

$$P_{il;jm} = \sigma_i^{col} \sigma_j^{col} \rho(|\vec{r}_i - \vec{r}_j|) \beta_{l;m}^{(ij)} \quad (1.3)$$

The term $\rho(|\vec{r}_i - \vec{r}_j|)$ is a homogeneous horizontal correlation function which depends only on the distance between the lat-lon positions i and j , and $\rho(0) = 1$. An advantage of the introduction of the superobservations is that the function ρ only needs to be computed for distances between model grid cells. Making use of the rotational symmetry of the globe, these function values can be pre-computed and stored in an efficient and relatively small lookup table.

The vertical covariances between the layers l and m and cells i and j are described by $\beta_{l;m}^{(ij)}$. The superscript indicates that the vertical covariance factors may still have a (weak) lat/lon dependence. If the quantities σ_i^{col} are normalized by setting $\sum_{lm} \beta_{l;m} = 1$ (note that this normalisation of $\beta_{l;m}$ is different from the normalisation for correlation matrices where the diagonal matrix elements are equal to one), then the term \mathbf{HPH}^T in 1.1 is

$$(\mathbf{HPH}^T)_{ij} = \sigma_i^{col} \sigma_j^{col} \rho(|\vec{r}_i - \vec{r}_j|), \quad (1.4)$$

where i and j are lat/lon indices of two grid cells that contain a superobservation. This implies that σ_i^{col} can now be interpreted as the uncertainty (in DU) of the model total column i .

In eq. 1.1 the analysis increments are distributed over the vertical levels with weight factors $w_l = \sum_m \beta_{l,m}$. These weight factors are normalised to $\sum_l w_l = 1$ (see above). The vector quantities w_l are the only variables needed in eqs. 1.3 and 1.1 and we do not need to specify the entire matrix $\beta_{l,m}$.

The total column observations, however, do not provide statistical information on these vertical weights w_l . In Jeuken et al. (1999) it was shown that the analysis results are not very sensitive to the choice of this distribution, as long as the analysis increments are small and have a small bias. We choose the actual tracer distribution for the scaling: $w_l = x_{i,l} / \sum_l x_{i,l}$. Between 10 and 1 hPa an additional reduction of the weights is applied and they approach zero above the 2-hPa level. This choice is based on the following arguments, which are particularly relevant for ozone, but also for methane it appears to be a good choice.

- The analysis produced with this choice has a minimal effect on the vertical profile shape, which is determined by the 3D model.
- A climatological, fixed profile shape gives rise to negative analysed ozone values near the tropopause, because of the low ozone concentrations and the steep increase in ozone just above the tropopause. Using the actual tracer-gas profile almost completely avoids the occurrence of negative values in the analysis.
- Above 10 hPa the chemistry timescale becomes very short. This implies that analysis increments will disappear rapidly, and the impact of the observations will be mostly lost. With our choice, ozone in the top layers is almost completely determined by the model, and assimilation increments are applied mainly below 10 hPa.

1.2.3 Covariance advection and error growth

The Kalman filter also describes the propagation of the forecast error covariance \mathbf{P} in time,

$$\mathbf{P}_{t+1} = \mathbf{M}\mathbf{P}_t\mathbf{M}^T + \mathbf{Q}. \quad (1.5)$$

\mathbf{Q} is the model error covariance, and describes the forecast error covariance increase related to model imperfections when the state is propagated one time step. This equation is the computationally demanding part in the Kalman filter: if the field is a vector with dimension N (the number of 3D grid cells), then the covariance matrix has dimension $N \times N$, and $2N$ times as many computations are involved in operating with the model on the covariance matrix. We avoid this computational problem by fixing the off-diagonal matrix elements of \mathbf{P} : the distance dependent correlation function $\rho(r)$ in Eq. 1.3 is taken to be time and space independent.

In a pure transport problem with zero \mathbf{Q} , the covariance is conserved in the Lagrangian sense. This means that the forecast error will be constant for air parcels following the flow. The transport of the model forecast error is therefore modelled by ($\sigma_i = \sqrt{P_{ii}}$)

$$\vec{\sigma}^{t+1} = \mathbf{M}\vec{\sigma}^t \quad (1.6)$$

In this equation σ is a 3D field. In eq. 1.3 we introduced a time and space dependent 2D forecast error σ^{col} , and this is related to the 3D field through the (unknown) vertical covariance $\beta_{l;m}^{(ij)}$. We approximate this relation by the assumption that the forecast error is transported like the tracer field. The field σ^{col} is distributed over the vertical proportional to the tracer amount in each layer. Then this 3D distribution is advected (eq. 1.6) and a new 2D column forecast error distribution is determined by integrating over the vertical levels. This approach conserves the forecast error (the forecast error summed over all grid cells is constant).

Apart from being advected, $\vec{\sigma}$ grows in time due to model imperfections, and a model error term (described below) is added to eq. 1.6.

1.2.4 Covariance analysis

The forecast error covariance decreases due to the new observations (new observations provide additional information and therefore result in a smaller uncertainty of the field at, and near to, the observations),

$$\mathbf{P}^a = \mathbf{P}^f - \mathbf{P}^f \mathbf{H}^T [\mathbf{R} + \mathbf{H} \mathbf{P}^f \mathbf{H}^T]^{-1} \mathbf{H} \mathbf{P}^f \quad (1.7)$$

This equation is replaced by an analysis equation in two dimensions, and is solved for the diagonal elements only,

$$(\sigma^{col,a})^2 = (\sigma^{col,f})^2 - \mathbf{B}^f [\mathbf{R} + \mathbf{B}^f]^{-1} \mathbf{B}^f \quad (1.8)$$

$$\text{where } B_{i;j}^f = \sigma_i^{col,f} \sigma_j^{col,f} \rho(|\vec{r}_i - \vec{r}_j|) \quad (1.9)$$

This can be viewed as the variance analysis equation for a 2D Kalman filter, with a 2D model for the trace-gas columns. Equation 1.9 can also be related to eq. 1.7 if the forecast error is assumed to be fully correlated between the vertical levels.

1.2.5 Parameter estimates

The error modelling described above defines several unknowns that can be estimated from the observation-minus-forecast (OMF) innovations.

- Horizontal error correlation

The horizontal error correlation was determined from the distance dependence of the correlation between the OMF innovations during a month of ozone assimilation. This led to the following functional form: $\rho(r) = (1 + r/L) \exp(-r/L)$, with a correlation length of 500 km ($L = 250$ km). For methane the same relation will be used.

- Observation error

In previous studies on ozone, the observation error was estimated indirectly, by optimizing the skill of the resulting forecasts. For GOME observations in combination with the model TM3DAM (see chapter 2), this resulted in $\sigma^{obs} = 5$ DU. For methane, the observation error will be derived

from estimates of the instrument sensitivity (see chapter 4).

- Model forecast error

In the Kalman filter equation 1.5 the model error covariance is often assumed to be uncorrelated in time. With this assumption the forecast covariance grows linear in time, and the forecast error grows like the square root of time. However, there is no justification for this assumption. Therefore, we have extracted the time dependence of the forecast error from the OMF statistics (see Eskes et al. 2002b). These statistics showed a characteristic steep increase of the forecast error, changing into a slow increase after 1-2 days. A reasonable parameterization of the time dependence is $(\sigma^f)^3 = \alpha t$, where the constant α depends on the month and on the latitude.

1.3 Conclusion

A scheme for the assimilation of satellite measurements of columns of trace gases has been described. The assimilation approach is based on the Kalman filter equations and provides detailed and realistic maps of the forecast error. Nevertheless, the scheme is computationally efficient. It is also flexible and can be used for arbitrary trace gases.

Chapter 2

Data assimilation of GOME ozone column data

This chapter gives a brief overview of the TM3DAM ozone data assimilation model. The parametrized Kalman filter approach, described in the previous chapter, is used to assimilate GOME ozone column data. The resulting ozone analyses and five-day ozone forecast data sets are provided via the GOME fast delivery web site.

2.1 Introduction

One of the first studies on ozone data assimilation is described by Levelt et al. (1996) where TOVS ozone data is assimilated with a simple 2D global model. With BCRS support, the KNMI has further improved and extended this ozone assimilation work (Jeuken et al. 1997; Eskes 1999; Eskes et al. 2001) in the last four years. These activities were directly related to the EU project SODA, "Satellite Ozone Data Assimilation" (Stoffelen et al. 1999). During the BCRS project "Sciamachy Data Assimilation", the TM3DAM data assimilation model was developed. The model aspect, assimilation approach and first results were presented in the report of this project (Eskes et al. 2001). Because of this, we will only give a short overview of TM3DAM in this chapter.

Within the second phase of the Sciamachy Data Assimilation project (described in this report) the operational processing of GOME ozone data was continued. This processing consists of 2 to 3 analysis and forecast runs, based on the latest ECMWF weather forecast and the latest *near-real-time* GOME ozone column data. A detailed paper was written on the model and assimilation aspects (Eskes et al. 2002b). Furthermore, a study was made on the forecast skill of TM3DAM (see next chapter) (Eskes et al. 2002a).

The modelling and data assimilation approach has several common aspects with developments

at other institutes. For instance, in Khattatov et al. (2000) the assimilation of Microwave Limb Sounder (MLS) ozone data with the ROSE chemistry-transport model is discussed. The Data Assimilation Office of NASA has developed the GEOS ozone data assimilation system for the off-line operational analysis of Total Ozone Mapping Spectrometer (TOMS) and SBUV-2 data, as described in Štajner et al. (2000).

2.2 Ozone modelling

The day to day variability in total ozone is first of all determined by (lower) stratospheric transport. Chemical time scales are typically longer, especially in the lower/middle stratosphere. Because the GOME satellite provides global coverage every three days, processes with time scales longer than a week are efficiently corrected by the assimilation of the ozone data. This provides the main motivation for the choice of the model: the main emphasis is on resolving the stratospheric transport with a good resolution. Ozone chemistry is approximated by parameterizations for gas phase and heterogeneous chemistry, which considerably reduces the computational cost.

2.2.1 Transport

The three-dimensional advection of ozone is described by the flux-based second order moments scheme. The model follows the new ECMWF vertical layer definition, operational from the end of 1999 until the present. The 60 hybrid layers between 0.1 hPa and the surface have been reduced to 44 by removing 16 layers in the lower and middle troposphere, and above 300 hPa the layers in the model coincide with the ECMWF layers. The horizontal resolution of the model version used in the operational processing is 2.5 by 2.5 degree. In the near future experiments will be performed for higher horizontal resolutions.

The model is driven by 6-hourly meteorological fields (wind, surface pressure, temperature) from the European Centre for Medium-Range Weather Forecasts (ECMWF) model. TM3DAM is used in both diagnostic and forecast mode. The diagnostic mode is driven by the archived six hour forecast (ECMWF first guess) fields. In forecast mode the model is driven by the results of the latest ten day forecast run performed at the ECMWF. In both modes the meteorological fields are updated every 6 hours.

2.2.2 Chemistry

Ozone chemistry is described by two parametrizations. One follows the work of Cariolle and Déqué and consists of a linearization of the chemistry with respect to sources and sinks, the ozone amount, temperature and UV radiation. A second parametrization scheme accounts for

heterogeneous ozone loss. This scheme introduces a chlorine activation tracer which is formed when the temperature drops below the critical temperature of polar stratospheric cloud formation. Ozone breakdown occurs in the presence of the activation tracer. The motivation for using chemistry parametrizations is first of all to reduce the computational cost. Secondly, the largest changes in ozone on the time scale of one day to a week are related mainly to transport. Even the dramatic ozone depletion occurring at the South Pole in August-September has a time scale of a week to a month. We found that the chemistry parametrizations provide a realistic simulation of the formation of the 2000 ozone hole.

2.3 Observations

The ozone analysis is based on total column ozone observations measured by the GOME instrument. A discussion of the ozone products and retrieval techniques can be found in Burrows et al. (1999). For ozone forecasting purposes a near-real-time product is essential. The data assimilation results described here are based on the fast delivery total ozone columns (Valks et al. 2002). The GOME measurements are collected and ozone columns are retrieval within 3 hours after the measurements are made. The width of the GOME swath is 960 km, divided in three pixels of 320 by 40 km, and the number of total ozone observations is about 18,000 per day. GOME has a global coverage in three days (apart from the dark winter pole).

2.4 Assimilation

The GOME observations are combined with the model with the parametrized Kalman filter data assimilation approach discussed in the previous chapter, and described in Eskes et al. (2002b).

2.5 Data sets produced

The processing of GOME data is performed operationally on a "best effort" basis. There is no 24h safeguarding of the processing, but when problems occur the group of scientist involved in the GOME processing will try to solve them during office hours. Up to three analysis/forecast runs are normally performed each day to account for the latest GOME measurements and ECMWF meteorological forecast.

The main product of the operational run are latitude/longitude total ozone fields which are available at 0, 6, 12, and 18 GMT. Secondly, each day a 12h local time (local noon) ozone distribution is produced. Based on these local-noon fields a clear-sky UV forecast is generated. The fields are stored in a data base (November 1999 – present) and the data can be requested as ASCII (TOMS format) data files and as images. Two internet tools have been developed for

specific data requests by users. These provide ozone column data at user specified locations and times. Monthly-averaged ozone maps are generated each month and are also available on the internet. The data is provided via the GOME Fast Delivery web site, http://www.knmi.nl/gome_fd (funded by the Data User Programme of ESA).

Apart from these products, the model produces statistics on the quality of the assimilation (the so-called observation minus forecast residuals) and detailed forecast error distributions. Ozone profiles at 122 ground stations are written to file every 6 hours. These data sets are used for intercomparisons with ground-based observations from Brewer, Dobson, Lidar and ozone sondes. These data sets will also be used to support the SCIAMACHY validation campaign.

2.6 Activities

The following activities have taken place during the Sciamachy Data Assimilation (phase 2) project:

- Monitoring of the TM3DAM operational ozone processing, to safeguard the availability of daily ozone analyses and forecasts.
- Several small improvements have been implemented in the TM3DAM code.
- The TM3DAM processing has been ported to the new SUN supercomputer at the KNMI.
- The number of computers involved in the operational chain has been reduced to improve reliability.
- The pre-processing at the ECMWF has been updated. TM3DAM now uses improved mass fluxes derived directly from the spectral vorticity and divergence fields (Segers et al. 2002).
- A re-analysis run has been performed for the period November 1999 – December 2000.
- The model is prepared for the assimilation of SCIAMACHY ozone data.
- Two papers have been written, one about the TM3DAM model and assimilation aspects, and one about the forecast performance (see next chapter).

Chapter 3

Ozone forecasts

In this chapter we present the forecast results of the TM3DAM ozone assimilation and forecasting system. TM3DAM is an ozone transport and chemistry model, driven by the operational medium range forecasts of the ECMWF. The forecast are initialised with realistic ozone distributions, obtained from the assimilation of near-real-time total column observations of the GOME spectrometer on ERS-2. The anomaly correlation and forecast error diagnostics demonstrate that the system produces meaningful total ozone forecasts for up to 6 days in the extratropics. In the tropics meaningful forecasts of the small anomalies is restricted to shorter periods of about two days with the present model setup. Important events, such as the breakup of the South Pole ozone hole and mini-hole events above Europe are successfully predicted 4-5 days in advance.

3.1 Introduction

Data assimilation is a well established essential component of numerical weather analysis and forecasts. Based on the available data of e.g. the past 6 hours, from satellite, balloon sounding, aircraft and other sources, and based on the model forecast, the most probable state of the atmosphere is reconstructed. This realistic analysis is the starting point for a (10 day) medium-range weather forecast.

The application of data assimilation in the field of atmospheric chemistry research is still new. This development was motivated by the experiences of numerical weather prediction centers, as well as by the available global data sets on ozone and other chemical species from satellite instruments. New satellite missions such as ENVISAT and EOS-AURA will provide huge volumes of detailed data on the 3D composition of the atmosphere. Data assimilation will play an important role to make optimal use of these future data sets.

A realistic modelling of the chemical state of the atmosphere is depending on the quality of the model (the description of atmospheric transport and the chemical reactions) but also on

the initial conditions (concentrations of especially long lived chemical species) and sources and sinks. Data assimilation uses the available data in an objective way to fix the initial state, which provides additional means to study the quality of the chemistry scheme and description of advection and convection in the model.

Ozone is an important trace gas for numerical weather forecast modelling. It has a strong influence on the temperature and dynamics in the atmosphere, and knowledge of ozone may improve satellite retrievals, especially the radiation modelling for the TOVS instruments. In the pioneering European Union project Satellite Ozone Data Assimilation (Stoffelen et al. 1999), techniques have been developed for the assimilation of ozone in several numerical weather forecast models, including the European Centre for Medium Range Weather Forecast (ECMWF) model. ECMWF ozone forecasts, based on near-real-time satellite ozone data, will become available in the near future. The National Oceanic and Atmospheric Administration (NOAA) has recently started to provide ozone forecasts based on assimilated operational Solar Backscatter UV (SBUV) data from the NOAA satellites. These activities can be seen as a first step towards a chemical forecasting system.

In this chapter we describe the quantitative results of an operational ozone forecasting system developed at the Royal Netherlands Meteorological Institute (KNMI), with support by the Netherlands Remote Sensing Board (BCRS). Apart from the forecast scores we will present two interesting examples: the breakup of the ozone hole and a recent ozone mini-hole over Europe. The system is based on GOME ozone data and a chemistry transport model driven by ECMWF forecasts of the meteorological fields. Daily ozone forecast, and a data base of ozone fields is provided via the web site of the KNMI, http://www.knmi.nl/gome_fd (Van der A et al. 2000). This work is done in the context of the ESA Data User Programme. Recently, ESA is mirroring the forecast results on the ESA portal <http://www.esa.int> (click on "Ozone Watch"). Furthermore, a global clear-sky UV analysis and forecast model has been coupled to the ozone forecasts.

3.2 The model and assimilation approach

The ozone forecasts are based on the tracer-transport and assimilation model TM3DAM, version 3. The modelling of the transport and chemistry, the GOME total ozone observations and the aspects of the ozone data assimilation were the topic of the previous sections. More detail can also be found in a recent paper (Eskes et al. 2002b) or the report of the Sciamachy Data Assimilation 1 project of the BCRS (Eskes et al. 2001).

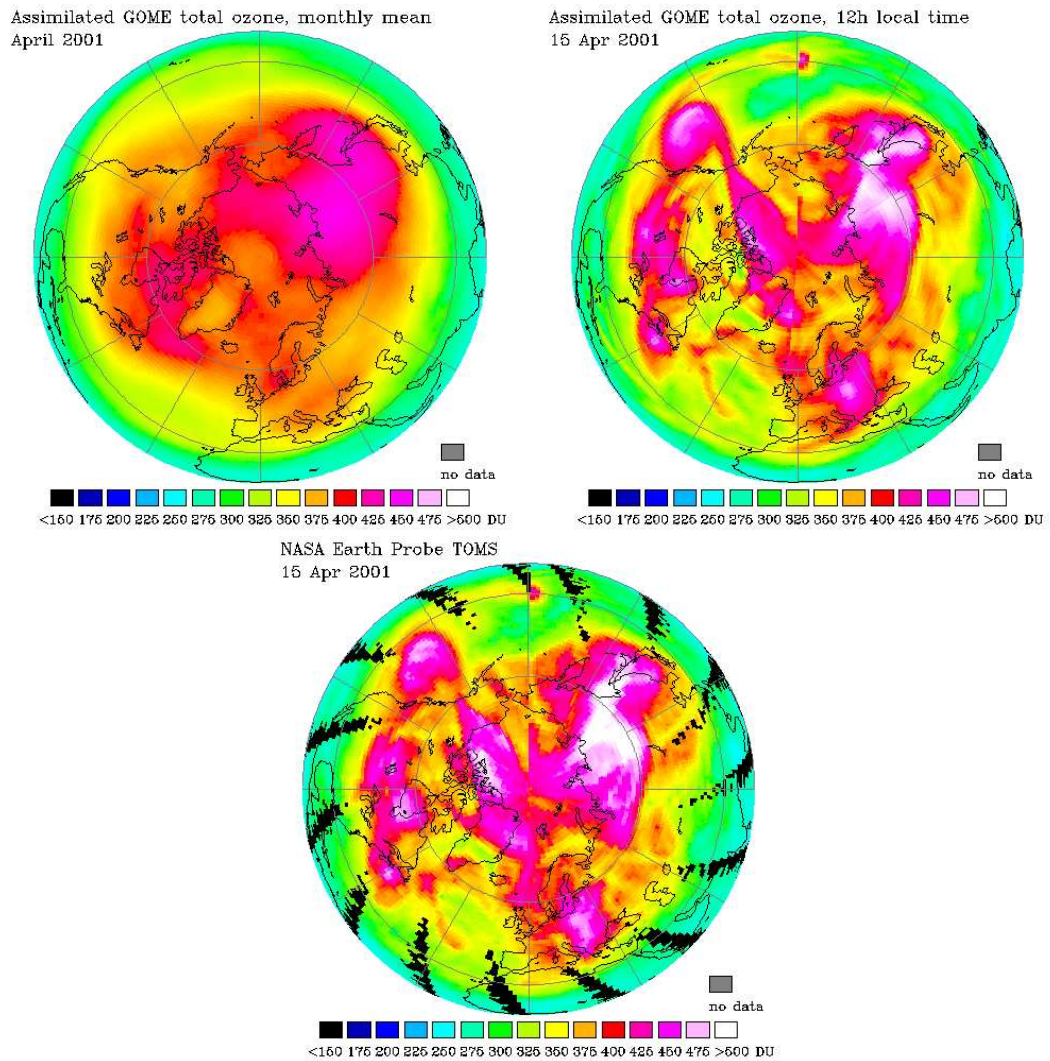


Figure 3.1: Total ozone distribution in the Northern hemisphere in April 2001. Top-left: monthly mean. Top-right: analysis on 15 April, 12h local time. Bottom: TOMS observations for 15 April. Scales in Dobson units.

3.2.1 Data assimilation results

An example of an ozone analysis produced by TM3DAM is shown in Fig. 3.1, right panel. For comparison, we show an Earth Probe TOMS map of ozone on 15 April 2001 in the lower panel (McPeters et al. 1998). TOMS has a nearly global coverage in one day, and the figure shows the ozone column observations gridded on a 1 by 1.25 degree grid. Because TOMS has a sun-synchronous orbit, we have constructed a 12 h local time global ozone map based on the model analysis (right panel).

As is clear from the figure, the agreement between TOMS and the TM3DAM assimilated GOME field is good. The small-scale features in ozone correlate very well with the small scale features in the TOMS map. The image provides an impression of the amount of detail in the assimilated ozone fields and the effective resolution of the model. On a larger scale there are also clear differences. These larger-scale differences can for a large part be attributed to differences in the instruments and the retrieval codes for TOMS and GOME.

On average the difference between new GOME observations and the short range model forecast (between 1 and 3 days) is small: about 9 Dobson Units (DU), or roughly 3 %. The bias between the model and the GOME columns is in general smaller than 1 %.

3.2.2 Operational ozone forecasts

Every day two or three forecast runs are performed with TM3DAM. Directly after completion of the 10-day forecast at the ECMWF (started at 12 GMT) the meteorological fields are extracted from the archive. The wind fields are converted in mass fluxes in a preprocessing step, and the data is sent to the KNMI by ftp transfer. Upon arrival an analysis and forecast run is started at the KNMI, based on the latest near-real-time GOME ozone data. Twelve hours later a new forecast run is performed, based on the same meteorological fields, but with an additional 12 hours of GOME measurements.

During the BCRS project "Sciamachy Data Assimilation, phase 2" several improvements were implemented to improve the reliability and modeling. A updated preprocessing software package was installed at the ECMWF. This update also contains the improved mass-flux calculation, as discussed in Segers et al. (2002). The number of computers involved in the preprocessing, file transfer and TM3DAM processing has been reduced to improve the continuity.

3.3 Anomaly correlation and RMS error

In numerical weather forecasting it is common practice to measure the performance of the medium-range forecast by plotting the anomaly correlation C_t (Simmons et al. 1995). Typically, anomalies of the 500 hPa height field are monitored (or wind field anomalies in the tropics). In

this paper we will investigate variations in the total column of ozone. The anomaly correlation is often defined as,

$$C_t = \frac{(f_t - c)(a - c)}{\sqrt{(f_t - c)^2(a - c)^2}} \quad (3.1)$$

Here c is the climatological value, i.e. a monthly mean (or better, daily mean) for a particular latitude and longitude. f_t is the forecast which was produced a time t before the verifying analysis a . The correlation C_t measures the correlation between the forecast anomaly ($f_t - c$) with a forecast time t and the analysis anomaly ($a - c$), both applying to the same time. c is the climatological value. The average is over forecast runs and over latitude/longitude.

The anomaly correlation in this form is not a very useful quantity for total ozone. An important assumption in 3.1 is that the climatological mean is well defined, and that $(a - c) \rightarrow 0$ for long averaging periods. This is not the case for ozone: there are considerable trends related to ozone depletion, there is a strong seasonal variation and a considerable year to year variation. Eq. 3.1, evaluated based on e.g. a 20 year climatology, will provide a too optimistic estimate of the forecast performance: persistent differences with respect to the climatology will have a positive contribution to C_t .

The left panel of Fig. 3.1 shows the monthly-mean ozone distribution for April 2001. Note that there is a pronounced zonal variation (wave 1). The monthly mean ozone maps also show a strong variability from year to year, e.g. the Northern Hemisphere ozone amount in April 2000 was about 20 DU smaller than in 2001. Given this variability we introduce a modified $C_t^{(m)}$ in which the anomalies are computed as the difference between the actual ozone column and a running monthly mean, i.e. the anomaly is the difference between the right and left panel in Fig. 3.1.

Fig. 3.2 shows the modified anomaly correlation as a function of the forecast time. The plot is based on approximately 9 months of forecast runs between December 2000 and January 2002. The top three curves correspond to the extratropical northern hemisphere (NH), the tropics (TR) and the extratropical southern hemisphere (SH). For comparison we also show the results for persistence (dotted curves). Persistence is calculated by keeping ozone fixed during the forecast period. Clearly the forecast runs are superior to persistence, which is only meaningful for a short time interval of about 1 day, when the anomaly drops below 0.6. We have also produced plots for the individual months, which all provide a very comparable behaviour to Fig. 3.2, although there is some variation from one month to another.

The SH and NH curves are a very encouraging result: after 5 days the forecast anomaly correlation is still well above 0.6. Extrapolation suggests that on average the forecasts are meaningful up to 6 days or even a bit longer. The current ECMWF meteorological forecasts are characterised by 500 hPa geopotential height anomalies that cross 0.6 after about 7 days, which is quite comparable to what we find for total ozone. Note that this crossing time is very sensitive to the choice of the climatological reference c (in our case a running monthly mean), and this dependence complicates the direct comparison between the ozone and height anomalies.

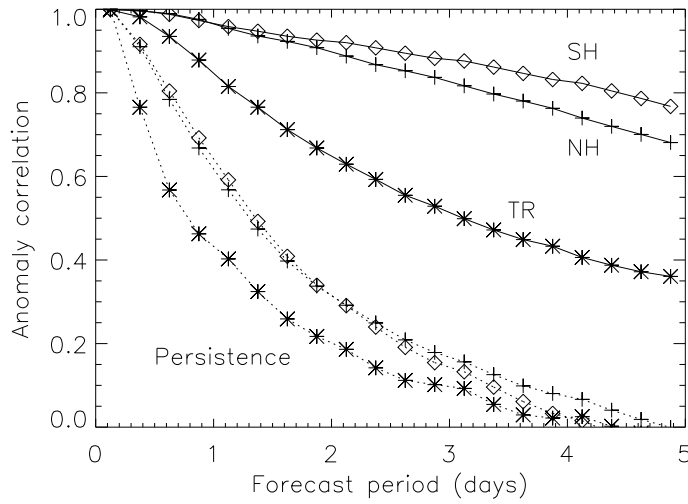


Figure 3.2: Modified anomaly correlation as a function of the forecast period. The top three curves represent the total ozone anomaly for latitudes north of 30 degree (NH), between -30 and 30 degree (EQ) and south of -30 degree (SH). The lower three curves are the scores for persistence.

The plot also suggest that the southern hemisphere has a somewhat better score than the northern hemisphere. This is a bit surprising. Traditionally the forecast skill of numerical weather prediction models has been better in the NH related to the dense observation network. In recent year this difference between the hemispheres in the ECMWF model has disappeared, and both sectors show good forecast skill up to 7 days. In the plots for the individual months there is a considerable spread in the comparison between NH and SH, ranging from $C_t^{(m)}$ in the SH being slightly lower than SH, to significantly higher (e.g. October 2001). A longer forecast data set is needed for more firm statements. The geographical distribution of $C_t^{(m)}$ shows also an interesting difference: for one particular month $C_t^{(m)}$ shows significantly more variation in the NH than in the SH. This difference may be related to orographic effects.

The forecast performance is systematically lower for the tropics. The value $C_t^{(m)} = 0.6$ is reached after about 2-2.5 days. The curves obtained shows very little seasonal variation: $C_t^{(m)}$ for a forecast time $t = 5$ days has a value between 0.32 and 0.42 for the individual months. There may be several reasons for this remarkable difference:

- 1) The ECMWF forecasts have generally been better in the extratropics as compared to the tropics. Again, in recent years there has been a considerable progress with the ECMWF model, and the differences in forecast skill have become small. Therefore it seems unlikely that this result is caused by a poor quality of the (horizontal) wind fields.
- 2) The (modified) anomalies are much smaller in the tropics than in the extratropics. For instance in November 2001 typical anomalies were 25, 8 and 22 DU in NH, TR and SH respectively. A value of 8 DU implies variations of the order of (only) 3 %. Near the equator the variation is even lower, about 2%. For such small anomalies the noise of the measurements will determine a large fraction of the anomaly, and will have a negative impact on the forecast

performance for these small anomalies.

3) The retrieval of ozone columns based on the GOME measurements is sensitive to aspects like clouds and surface albedo. Clouds make the below-cloud ozone column invisible. The retrieval approach corrects for this cloud effect by adding a climatological below-cloud ozone "ghost" column to the retrieved ozone column. Additional information on cloud fraction and cloud top height, derived from the GOME data, is used for this. Such cloud-related biases will have a negative effect on the skill.

4) Most of the ozone column variation in the tropics can be attributed to the troposphere. This in contrast to the extratropics, where the lower stratospheric dynamics is responsible for the large ozone column variabilities observed. The model, however, does not describe tropospheric chemistry: the two chemistry parametrizations are applied in the stratosphere only.

The small anomalies in combination with the measurement noise, retrieval errors and model deficiencies will be the main reason for the large contrast between the tropics and the extratropics. Note also that persistence in the tropics performs considerably worse than persistence in NH and SH. This suggests that there is additional "noise" that influences the results, or that the characteristic length scale/time scale is much smaller in the TR sector than in the NH, SH sectors.

Another interesting feature is revealed by global maps of the anomaly correlation. This shows an interesting zonal behavior in the ± 15 degree latitude belt along the equator. Over the Pacific $C_t^{(m)} \approx 0.3 - 0.6$, while over the Atlantic $C_t^{(m)} \approx 0 - 0.2$. This correlates well with the zonal variation of the tropospheric ozone column (see, for instance, Fishman et al. 1990), which shows a pronounced maximum over the Atlantic ocean due in particular to biomass burning pollution. This difference suggests that with a realistic modelling of tropical tropospheric ozone the forecast skill in the tropics can be improved.

As mentioned above, the modified anomaly correlation is very sensitive to the choice of the climatological reference. An alternative measure of the forecast skill which is less sensitive to the climatological mean is the root mean square (r.m.s.) error. A normalised r.m.s. error E_t for a forecast time t is defined by,

$$E_t = \frac{\sqrt{(f_t - a)^2}}{\sqrt{(a - \bar{a})^2}} \quad (3.2)$$

This quantity directly measures the r.m.s. difference between the forecast and the verifying analysis. The denominator compares this forecast minus analysis difference with the ozone variation of the analysis. For long forecast times we may assume that the forecast and analysis anomalies become uncorrelated. If the model is not lazy, i.e. if the forecast and analysis show the same range of ozone values, then $E_t \rightarrow \sqrt{2}$ when $t \rightarrow \infty$. This r.m.s. error is plotted in Fig. 3.3. The curves for E_t show a near linear behaviour with the forecast time for the NH and SH. In the first day a larger r.m.s. error growth is found. These results are quite similar to the geopotential height r.m.s. error curves found for the ECMWF model. Consistent with figure 3.2 E_t is considerably larger in the tropics.

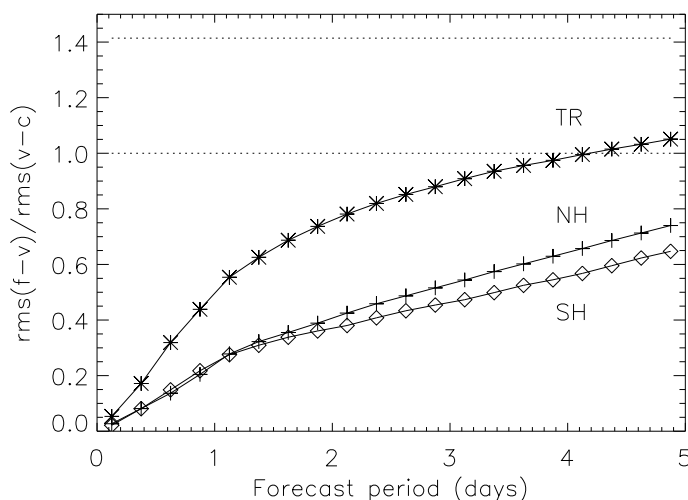


Figure 3.3: Root-mean-square of the difference between the forecast and the verification, normalised with the ozone column variation. The three curves are for latitudes north of 30 degree (NH), between -30 and 30 degree (EQ) and south of -30 degree (SH).

3.4 Ozone forecast examples

In this section two prominent examples of ozone forecasts will be discussed.

3.4.1 The year 2000 ozone hole

The rapid depletion of ozone in August/September over the South Pole is governed by heterogeneous chemistry processes. In contrast, the development of the ozone hole and the recovery of the ozone layer in November/December is related mainly to dynamical aspects and the polar vortex becoming unstable. The year 2000 was quite exceptional, with a rapid development of the ozone hole in August and an early recovery in mid November.

Fig. 3.4 shows the 4-day forecast that was produced on 15 November, together with the analysis fields for 15 and 19 November. The initial field (left panel) shows the ozone hole displaced in the direction of Africa. By this time the ozone layer has already recovered significantly and the area of the depleted region is a factor of 3 smaller than in early September. The forecast run performed on this day (right panel) predicted a breakup of the hole. Almost half of the depleted air is predicted to mix with mid-latitude air, resulting in a significant lowering of midlatitude ozone below Africa. A smaller part of the depleted air is predicted to move in the direction of New Zealand. This prediction is essentially confirmed by the verification on 19 November, with a slightly different partitioning of the air masses.

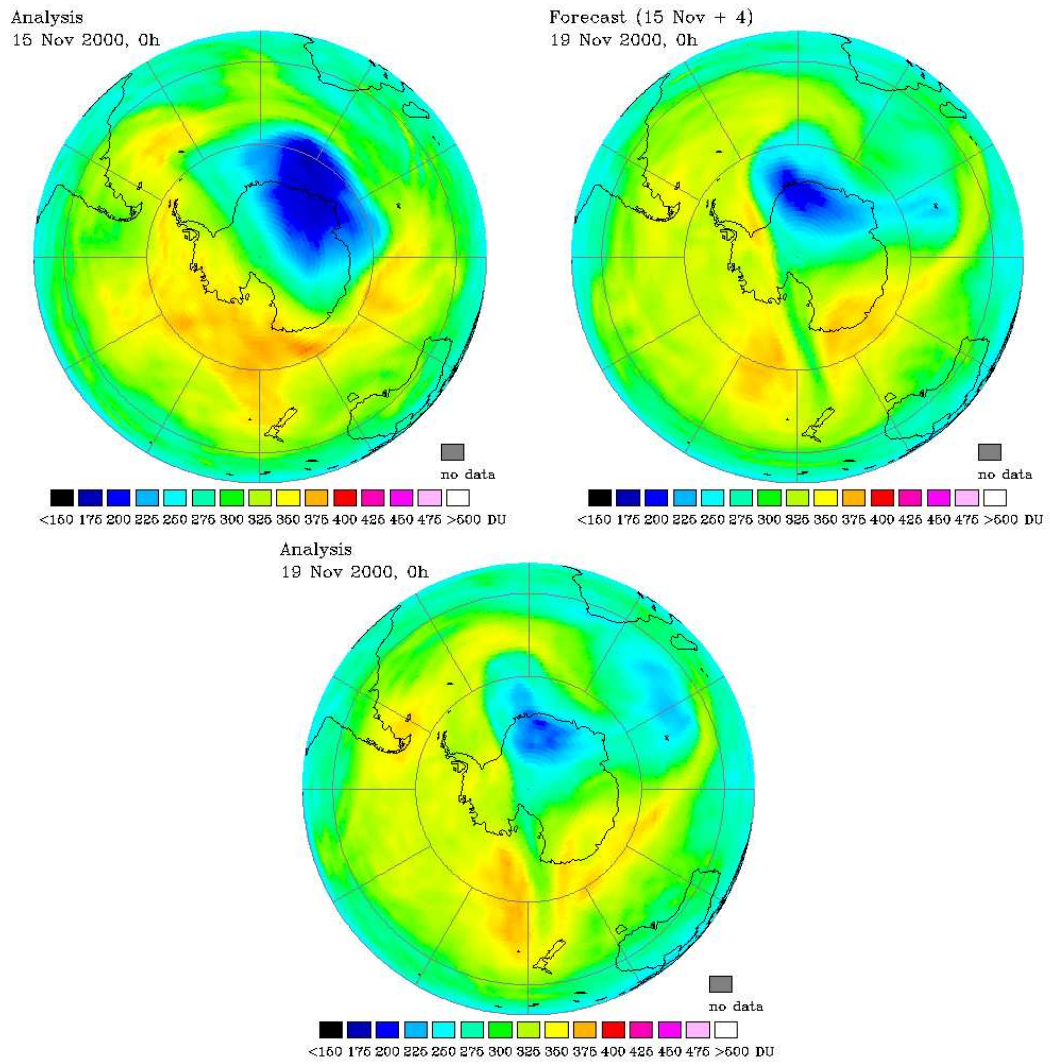


Figure 3.4: The final days of the 2000 ozone hole. Top-left: Southern Hemisphere ozone on 15 November 2000. Top-right: four day forecast for 19 November. Bottom: verification on 19 November.

3.4.2 Low ozone episode over northern Europe

Low ozone events (ozone mini-holes) over Europe have attracted considerable attention recently. In November 2001 a series of such events occurred. Ozone miniholes often occur over the Atlantic and Northern Europe. The lowest ozone values remain only about 1-2 days, and these events are mainly of dynamical origin, with transport of air with low ozone mixing ratios from the subtropics to higher latitudes.

Figure 3.5 shows a forecast of the first large low ozone event of the winter 2001-2002. The five-day forecast (left panel) predicted a thin ozone layer above Iceland and the Atlantic, in qualitative agreement with the analysis and the GOME data 5 days later. Also the ozone patterns agree well with the verifying analysis. The three days forecast predicted even lower values at essentially the same location, and this forecast is very close to the observations on 9 November with minimum ozone values below 200 DU.

3.5 Conclusions

To summarise, the results of the TM3DAM ozone data assimilation and forecast system have been presented. The system is based on a transport-chemistry model driven by ECMWF meteorological forecasts, and assimilates near-real-time total column ozone measurements of the GOME spectrometer. The ozone analysis produced is realistic, and the detailed ozone distribution compares favourably with independent ozone observations from TOMS. The short-range forecast that is part of the analysis show a small bias (generally $< 1\%$) and is able to predict the new GOME observations with a precision of about 3% globally averaged.

Based on these ozone analyses, 5-day ozone forecast runs are performed routinely, and the quantitative performance of this forecast system has been presented. The results, collected over the period between December 2000 and January 2002, demonstrate that medium range ozone forecasts can be performed with a quality similar to geopotential height anomaly forecasts. The (modified) anomaly correlation in the extratropics crosses the value of 0.6 after about 6 days with the present setup, and therefore meaningful ozone forecasts can be produced for a period of almost one week. In the tropics the anomaly statistics is significantly worse, and we attribute this to a combination of the size of the anomaly in the tropics (r.m.s. only 2-3%), uncertainties and noise in the observation and retrieval code, and the lack of tropospheric chemistry in the model. Improved results are anticipated for model with a realistic description of tropospheric chemistry. It was shown that extreme events such as ozone mini-holes can be forecasted successfully 4-5 days in advance.

A natural extension of the ozone forecasts is a forecast of the (clear-sky) UV index. This extension has been implemented in the context of the GOME Fast Delivery Service, an ESA Data User Programme project (http://www.knmi.nl/gome_fd). Ozone forecasts have a wide range of applications, including:

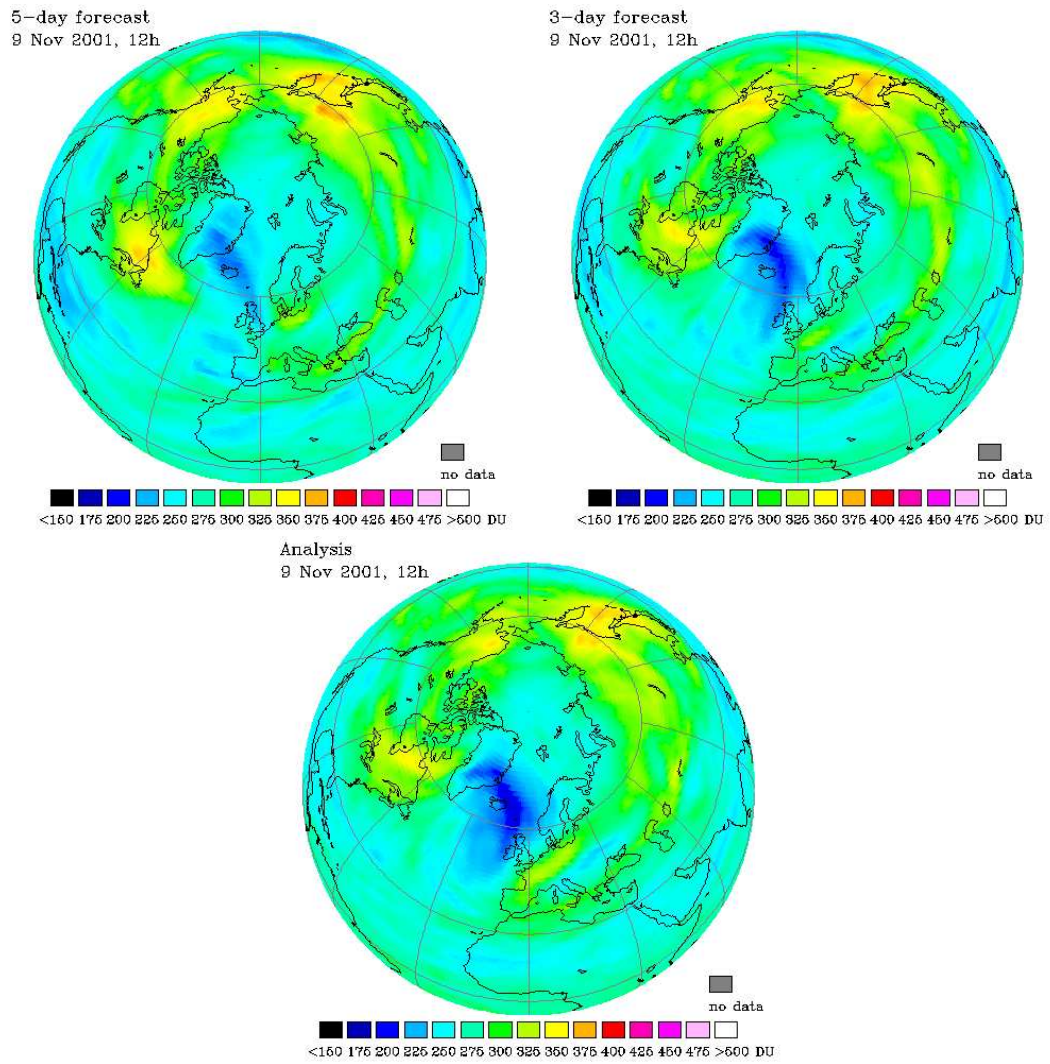


Figure 3.5: The first large ozone hole of the winter 2001-2002, on 9 November 2001. Top-left: 5-day forecast. Top-right: 3-day forecast. Bottom: verification.

- UV forecasts
- UV warnings (e.g. in case of excursions of the ozone hole over South America)
- prediction of special events, e.g. breakup ozone hole, low ozone events (ozone mini-holes)
- planning of measurement campaigns, validation activities.

Numerical weather prediction centers, such as NOAA-NCEP and ECMWF, have started activities to assimilate ozone data from operational and research satellite instruments. In the coming years we can expect ozone forecast products of similar or better quality than the system described here. A natural future extension of these activities is stratospheric and tropospheric chemical weather forecasting, which can be achieved by coupling more extended chemistry schemes to NWP models and by the assimilation of new observations of the chemical composition of the atmosphere as provided by satellite missions such as ENVISAT and EOS-AURA.

Chapter 4

Assimilation of methane satellite data in a tracer transport model

In this chapter the TM3/TMSCIA model is used for simulating methane globally. First, some results of multi-year runs on coarse grid are presented. Subsequently, a single-tracer version for CH₄ is developed. This version is coupled to the data-assimilation system described in chapter 1. As a first test, synthetic satellite observations of CH₄ columns are assimilated for a period of one month. The assimilation works well and will allow to create global fields that are consistent with future SCIAMACHY measurements.

4.1 Introduction

An important reason to study methane (CH₄) is that it is the second most important anthropogenic greenhouse gas, after carbon dioxide (CO₂). Since pre-industrial times (say 1750 AD) the observed (from ice cores) 150% increase in the globally averaged CH₄ abundance has resulted in an estimated global radiative forcing of about 0.5 W m^{-2} , which is about 20% of the radiative forcing by all greenhouse gases together (IPCC 2001).

CH₄ molecules heat the lower troposphere by gaseous absorption of terrestrial radiation in atmospheric windows. Windows are parts of the spectrum where the absorption by water vapour (H₂O) is small. While the CH₄ increase heats the troposphere, it tends to cool the stratosphere, although in an indirect way: oxidation of CH₄ by OH radicals produces extra H₂O in the dry stratosphere which enhances the stratospheric cooling to space.

CH₄ contributes most to the integral infrared atmospheric absorption in a band centered around $7.66 \mu\text{m}$ (1304 cm^{-1}). Changes in the outgoing longwave radiation (OLR) at the top of the atmosphere in response to the observed changes in the greenhouse gases have been observed by differencing satellite measurements of the spectral OLR between 7 and $14 \mu\text{m}$ made in 1970

and 1997, respectively (Harries et al. 2001). These measurements corroborate the radiative forcing of the global atmosphere by increased CH₄ concentrations.

Unlike CO₂, the radiative forcing by CH₄ depends on the atmospheric chemistry. CH₄ oxidation takes place mainly in reaction with the highly variable OH radical. The OH radical is in continuous chemical interaction with its environment and depends primarily on the solar UV radiation intensity between 300 and 325 nm, the concentrations of O₃ and H₂O, and on the emissions and abundance of CO and (partially oxidised) hydrocarbons and nitrogen oxides (NO_x = NO+NO₂). Most oxidation of CH₄ takes place in the humid boundary layer and in the lower troposphere.

In order to simulate the global CH₄ distribution atmospheric models need to incorporate the CH₄ sources, atmospheric transport and chemical loss. The sources and their strengths need to be identified and the modelled concentration distribution needs to be verified. Therefore, there is a strong demand to measure the global distribution of CH₄ and to locate and quantify its major sources.

The global CH₄ column distribution is measured by 'SCIAMACHY' (Bovensmann et al. 1999). SCIAMACHY stands for 'Scanning Imaging Absorption Spectrometer for Atmospheric Cartography'. It is a UV-VIS-near-IR spectrometer measuring reflected sunlight. The instrument has been launched the 1st of March 2002 on the ESA platform ENVISAT. The SCIAMACHY CH₄ column measurements are unique in their coverage and expected accuracy. Most present-day satellite measurements of CH₄ are limited to stratospheric profiles such as from HALOE/CLAES instruments on board of the UARS platform launched in 1991 and from MIPAS on board of ENVISAT.

Column amounts of CH₄ have only been measured in the thermal infrared by IMG on ADEOS-1 in 1996-1997 and in the near-infrared by MOPITT on EOS-TERRA. However, so far no CH₄ column data have been published from these instruments mainly due to algorithm and instrumental problems. Next to SCIAMACHY also IASI on METOP (launch 2006) and TES on EOS-AURA (launch 2004) will measure the CH₄ column in the near future. However, SCIAMACHY is the only instrument with spectrally resolved measurements in the near-infrared region and therefore SCIAMACHY is more sensitive to methane variations in the planetary boundary layer than the outgoing radiation in the thermal infrared region. Given the expected accuracy of the SCIAMACHY measurements, these data have the potential to help characterising the CH₄ global distribution

The satellite measurements may also help to improve our knowledge on the geographical and temporal distribution of CH₄ sources. The spatial integrations of satellite measurements are over large atmospheric domains (30 × 240 km² pixel size for SCIAMACHY) and are repeated every few days. These sampling characteristics largely overcome the problem of representativeness of the traditional methane observations for source characterization faced in inverse modelling studies using methane surface measurements in background air (Houweling et al. 1999), in the analysis of aircraft measurements (Beswick et al. 1998), and in the upscaling of

local methane emission measurements in the surface layer to landscape size ($10\text{--}10^4\text{ km}^2$) due to the inhomogeneous character of the emissions (e.g., Beswick et al. 1998).

The continuous time series of the satellite measurements allows to follow air masses and their evolution such that regional and global methane budgets can be constructed from landscape to continental size and from time scales of days to 1–2 months. The best method for these type of investigations will be to confront the column observations with model simulations by means of data assimilation.

The first studies in this direction were performed in the BCRS project MEGGY (Roemer et al. 2001a;b). This project comprised the development of the TMSCIA version of the TM3 tracer transport model. Inverse modelling techniques were used to relate (synthetic) methane satellite observations to surface emissions. A major outcome of MEGGY was the feasibility to use SCIAMACHY methane observations for emission detection on continental scales as long as the uncertainty in the retrieved column densities is very low: 1–2% at the most.

In the present study, synthetic satellite observations of methane column amounts are assimilated into a single-tracer version of TMSCIA. Error estimates according to Roemer et al. (1996) are used to provide a best-case uncertainty measure for these observations (the final uncertainty in the column amounts is not yet known). The ability of the assimilation system to adapt to the measurements is investigated. This gives a good indication of what can be expected when SCIAMACHY data will become available. An important aim of this work is to assist in the SCIAMACHY validation activities within the COMETH (Validation of CO and METHane SCIAMACHY data products) project.

4.2 Current status of knowledge on methane

Since characterization of the emissions is a crucial prerequisite for CH_4 modelling, a short overview of current knowledge on these emissions is given. Then the status of atmospheric models and their capability of simulating global distributions of methane is outlined. Multi-year runs with the TM3 model have been performed by Dentener et al. (2002), in close collaboration with the present project.

4.2.1 Emissions

The total global CH_4 emission rate is relatively well established and based on both bottom-up estimates based on socio-economical parameters (Olivier et al. 1996) (Van Aardenne et al. 2001) and (inverse) modelling studies using methane surface measurements in background air (e.g., Houweling et al. 1999; Dentener et al. 2002). However, much less is known about the geographical distribution of the methane sources, source characterisation, and possible temporal variations on a global and regional scale.

The estimated present-day global annual CH₄ emissions sum to around 575 (± 50) Tg per year (Houweling 2000; IPCC 2001). Global methane emissions are estimated to stem for about 1/3 from wetlands and other natural sources, while about 2/3 is assumed to be related to anthropogenic activities. The largest anthropogenic sources include fossil fuel production and consumption (≈ 90 Tg), domestic ruminants (≈ 90 Tg), and rice cultivation (≈ 80 Tg), with smaller contributions from biomass burning (≈ 50 Tg), waste treatment (≈ 50 Tg), and minor sources.

Given a globally averaged CH₄ concentration of 1745 ppbv in 1998 (IPCC 2001) and a global atmospheric CH₄ burden of 4850 Tg ($\pm 5\%$), the globally averaged CH₄ column is about 9.5 ± 0.5 g CH₄ m⁻², or in Dobson Units (DU): 1330 ± 70 DU (1 Dobson Unit equals 10⁻³ cm atm). The calculated chemical lifetime for CH₄ in the present-day atmosphere is about 8.4 ± 0.8 years.

Since pre-industrial times (say 1750 AD) the observed 150% increase in the globally averaged CH₄ concentrations has resulted in an estimated global radiative forcing of about 0.5 W m⁻², which is about 20% of the radiative forcing by all greenhouse gases together (IPCC 2001). The methane trend is about 0.5% per year, however with large interannual variations (Dentener et al. 2002). The methane trend is slowly decreasing for reasons that are not well understood. The diminishing growth rate might be related to decreasing emissions (either natural or anthropogenic) as well as to increasing oxidation efficiency.

4.2.2 Model simulations

From multi-year model simulations it is learned that, although the observed increase in the CH₄ concentrations since pre-industrial times is primarily due to increased CH₄ emissions, a significant secondary contribution to the methane increase is due to a reduction of its oxidation. The increased CH₄ concentration has increased the competition for OH radicals, which reduces the oxidation per CH₄ molecule (positive feedback). Based on an intercomparison between five chemical transport models with full photochemistry it has been estimated that, in the present day atmosphere, a methane emission increase is amplified by a factor in the range 1.34 to 1.63 due to reduced methane oxidation (Karlsdóttir 2000). The exact value of the positive feedback depends on several parameters. Except for the CH₄ concentration the two most important parameters are probably the emissions of CO and NO_x. The role of CO is mainly its competition with CH₄ for reaction with OH, i.e., higher CO concentrations reduce the availability of OH for reaction with CH₄ and therefore increase CH₄ lifetime. The role of NO_x is to enhance the number of oxidation cycles to which one OH molecule can contribute before it is irreversibly converted to a stable compound (Warneck 1988). Therefore, higher NO_x concentrations typically promote CH₄ oxidation. Gupta et al. (1998) have shown that especially a redistribution of NO_x emissions from mid-latitudes to tropical regions is expected to increase CH₄ oxidation. This is a likely scenario for the past decade in which emission control in Western Europe and the USA has been accompanied by rapid industrialisation in developing countries closer to the

Equator. Somewhat unexpectedly a redistribution of CO emissions and even of CH₄ emissions will have less impact on the CH₄ oxidation and lifetime.

On timescales of years the response of CH₄ concentrations to changes in CH₄ emissions is difficult to predict. Full chemistry-transport models are needed to study the response to emission changes, taking into account that the atmosphere is not in chemical equilibrium and the response time might even exceed the methane lifetime (Prather 1994). Changes in the chemical feedback processes are likely to be responsible for at least part of the observed variability in methane growth rate over the past 20 years, next to possible changes in the methane sources (Dlugokencky et al. 2001).

Multi-year simulations have been performed with the TM3 model (version TMSICA, see section 4.3) to examine the trend and interannual variability of methane emissions. The anthropogenic emissions of CH₄ and also NO_x, CO, NMHC, SO_x, and NH₃ for these runs are taken from the emission database developed by Van Aardenne et al. (2001). This database, which is based on the widely used EDGAR emission database (Olivier et al. 1996), describes the development of emissions during the period 1890-1990. Emissions after 1990 are obtained by extrapolation of the 1990 emission using CO₂ emission statistics obtained from Marland et al. (2000). The natural emissions of methane are prescribed following Houweling (2000).

Figure 4.1 (F. Dentener, personal communication) shows the comparison between modelled and measured methane trends at some remote surface stations from the NOAA CMDL network. The figures illustrate the capability of the model to simulate the background methane concentrations, i.e. far from the source regions. Note that in the simulations the surface concentration distribution of methane was fixed and a trend to the surface concentrations was applied based on the observed trend at the South Pole station. The main conclusions that could be drawn from the simulations was that the interannual variation of the global methane source strength is about 8 Tg CH₄, and most likely related to mid- and low-latitude wetland emissions and/or biomass burning (Dentener et al. 2002). The calculated trend in methane emissions over the 1979–1993 period is 2.7 Tg CH₄ per year.

4.3 The TM3 model, version TMSICA

TM3 (Tracer Model 3) is a global atmospheric chemistry–transport model, on the basis of which the version TMSICA has been developed. This version has specifically been designed for the interpretation and simulation of SCIAMACHY-derived columns and profiles of trace gases in the troposphere and lower stratosphere. The model is driven by six-hourly mean meteorological fields from ECMWF (Van Velthoven and Kelder 1996) and contains EDGAR emission estimates (Olivier et al. 1996). The model version applied in this study is basically the same as described in Lelieveld and Dentener (2000). However, an important difference is that in this study fixed methane *concentrations* were imposed at the surface, whereas here methane *emissions* are included following Houweling (2000).

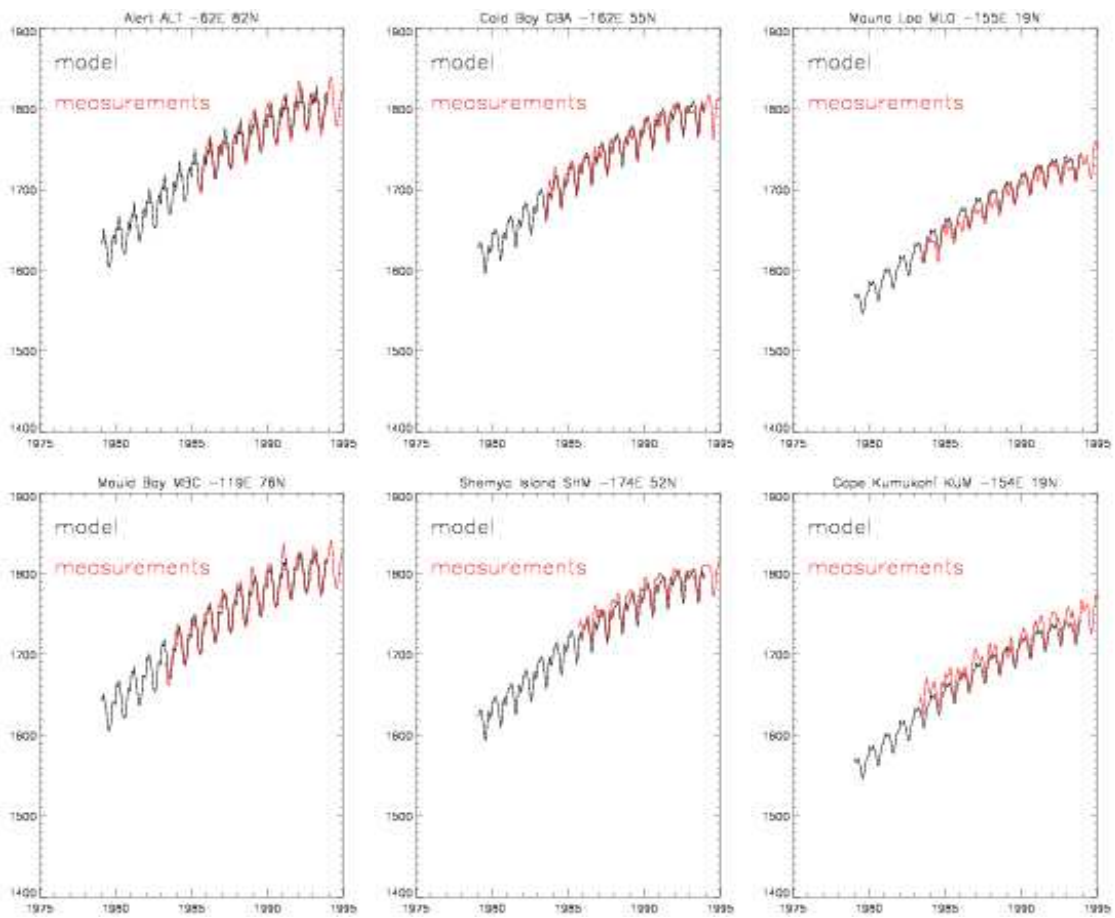


Figure 4.1: Comparison of model simulations with surface measurements of methane at six different locations for the ERA-15 period.

In the previous section, TMSCIA was applied with a course horizontal resolution of 10° longitude and 7.5° latitude for testing the long-term modelling capabilities for methane. In the following, we focus on a period of one month (July 2000), for which the model is run on a much finer resolution of $2.5^\circ \times 2.5^\circ$. The course-grid simulations had 19 levels in the vertical, while the fine-grid simulations use 31 levels. The vertical levels are defined with a hybrid from terrain-following sigma coordinates near the surface to pressure levels in the stratosphere, extending up to 10 hPa.

Tracer advection is done with the slopes scheme of Russell and Lerner (1981). Convective tracer transports are calculated with a mass-flux scheme that accounts for shallow, mid-level and deep convection as by Tiedtke (1989). Turbulent vertical transport is calculated by the stability-dependent vertical diffusion scheme following Louis (1979). Photolysis rates are calculated with a parameterized radiative transfer scheme at seven characteristic wavelengths (Krol and Van Weele 1997; Landgraf and Crutzen 1998). Dry deposition is parameterized as in Ganzeveld et al. (1997), while for wet deposition the parameterization by Guelle et al. (1998) is used. The chemical scheme includes tropospheric CH_4 -CO-NMHC- NO_x - SO_x chemistry and accounts for 38 species, of which 15 are transported, 24 photolysis reactions, and 67 thermal reactions (Houweling et al. 1998). The time steps for transport and chemistry depend on the resolution: 90 minutes for the course grid and 30 minutes for the fine grid.

At the top of the model domain, the concentration of a number of tracers is relaxed to climatology. Methane concentrations at the highest model level are nudged to the monthly-mean zonal HALOE/CLAES climatology from UARS. Similarly, the ozone concentrations above 50 hPa (i.e. at the upper three levels) are relaxed to the zonal-mean ozone climatology of Fortuin and Kelder (1998) scaled with Earth-Probe TOMS monthly-mean zonal ozone columns for 2000. Finally, monthly-mean HNO_3/O_3 ratios at 10 hPa from HALOE/CLAES are used to determine stratospheric HNO_3 levels. The stratospheric destruction of methane by reaction with OH, Cl, and $\text{O}(^1D)$ is taken into account by loss-rate factors that give the total CH_4 loss relative to the loss due to OH. These factors have been calculated at RIVM using a 2-D model.

4.3.1 Simulation for the present case

When assimilating satellite data we are interested in relatively short timescales (days/weeks) rather than in monthly averages. For the present study the month July 2000 has been selected. The TM3/TMSCIA model has been run on a high resolution for this month. Figure 4.2 shows the emissions on the fine grid as they are used in the current version of TM3/TMSCIA, described above. The bottom panel of figure 4.2 shows the monthly mean columns of methane as predicted by the model. These depend strongly on the surface pressure (see also Roemer et al. 2001b). To remove this dominating orographic effect, the columns have been divided by the local surface pressure and multiplied by the globally-averaged surface pressure (985 hPa). The areas where the main emissions take place can be recognized in the column distribution, but it should be noted that the variability in emissions is much larger than in the column amounts.

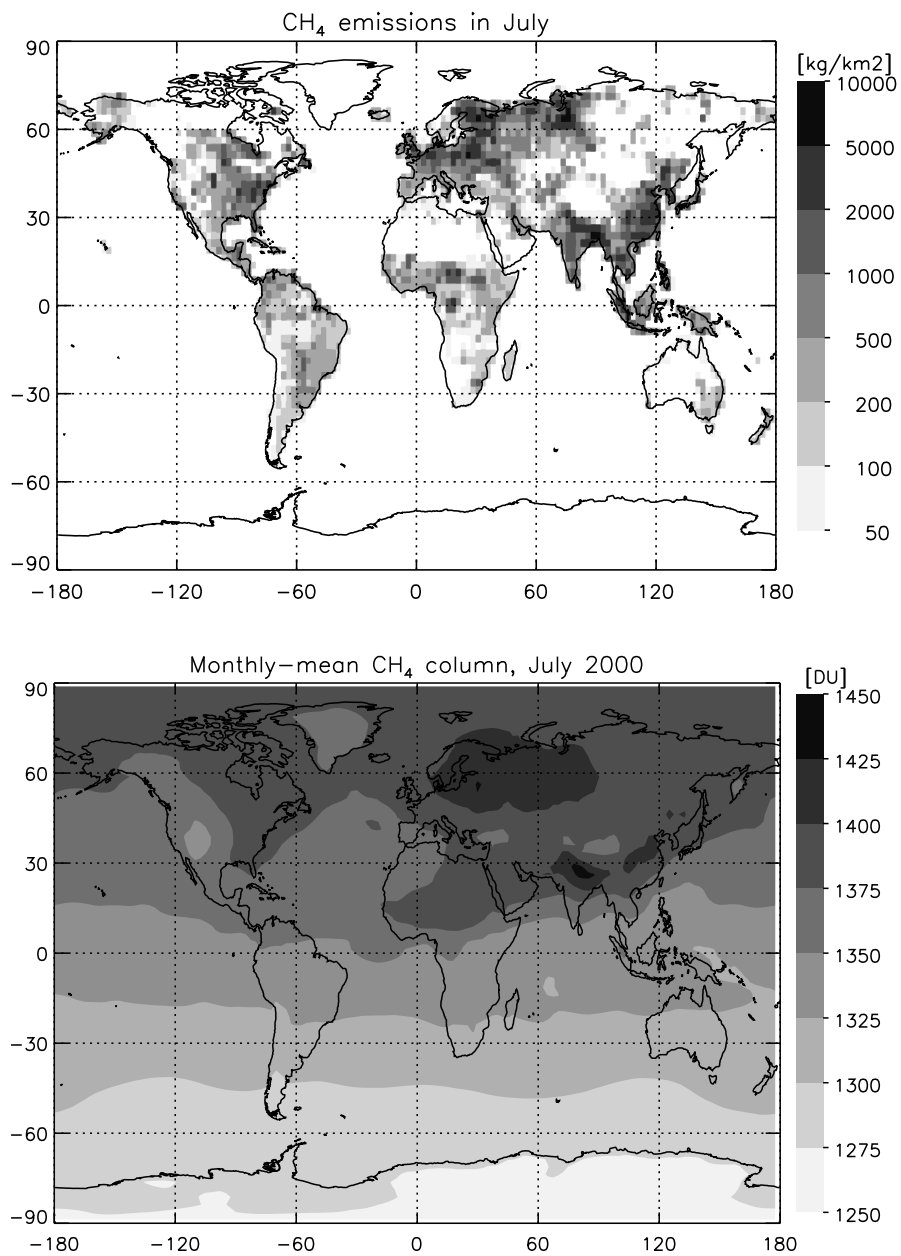


Figure 4.2: Top: methane emissions in July (note the logarithmic scale). Bottom: monthly-mean methane column distribution scaled with local surface pressure.

In the MEGGY project, mentioned before, the relation between emissions and column amounts was analyzed in detail. It was concluded that emission enhancements of 50% give rise to 1–2% (around 20 DU) column enhancements, which indicates that satellite measurements of methane should have this accuracy, before they can be linked to surface emissions.

4.3.2 Methane single-tracer version

In the project a single-tracer version of TM3/TMSCIA was developed. It is relatively simple to make such a stripped version for CH₄ because the only interaction with other species comes from the reaction with OH. To take this reaction into account, OH fields based on a run with the full-chemistry version are used. In order to resemble the diurnal cycle of OH, these OH fields are monthly averages of three-hour periods. As a result, eight fields per month are stored.

In a forward run, the differences between the stripped and full-chemistry versions should remain small. This is indeed the case, as can be seen in figure 4.3 (top panel). After a one-month run, the difference in column amounts is on average 0.5 DU, which is 0.04%, and maximum around 2 DU. The difference is highest near the surface (up to 0.07%). The bottom panel of figure 4.3 shows that taking the loss due to OH into account is necessary. The differences with the full-chemistry version are in this case up to 45 DU (3–4%), which is unacceptable. Note that the largest effects of oxidation are present on the Northern hemisphere, where the formation of OH is favoured by higher concentrations of O₃ and NO_x.

The importance of taking into account the daily variations of OH by storing 8 fields was also checked. It was found that when this is not done, slightly worse CH₄ fields are obtained. In particular, the CH₄ concentration is over- (under-) estimated towards the end of the day (night). It thus appears worthwhile to take the daily cycle into account.

4.4 Assimilation

In this section a data-assimilation experiment is outlined. Synthetic satellite measurements are created for the month July 2000. Subsequently, these measurements are assimilated into the single-tracer version of TMSCIA. The data-assimilation scheme used here is as described in chapter 1. For the moment, the error modelling is not performed; a simple fixed-error scenario is chosen.

4.4.1 Generation of synthetic data

Synthetic satellite observations are created for GOME tracks. This is a reasonable choice since SCIAMACHY and GOME have the same swath (960 km). A difference, however, is that SCIAMACHY switches between limb and nadir mode every minute. Thus, the coverage is only

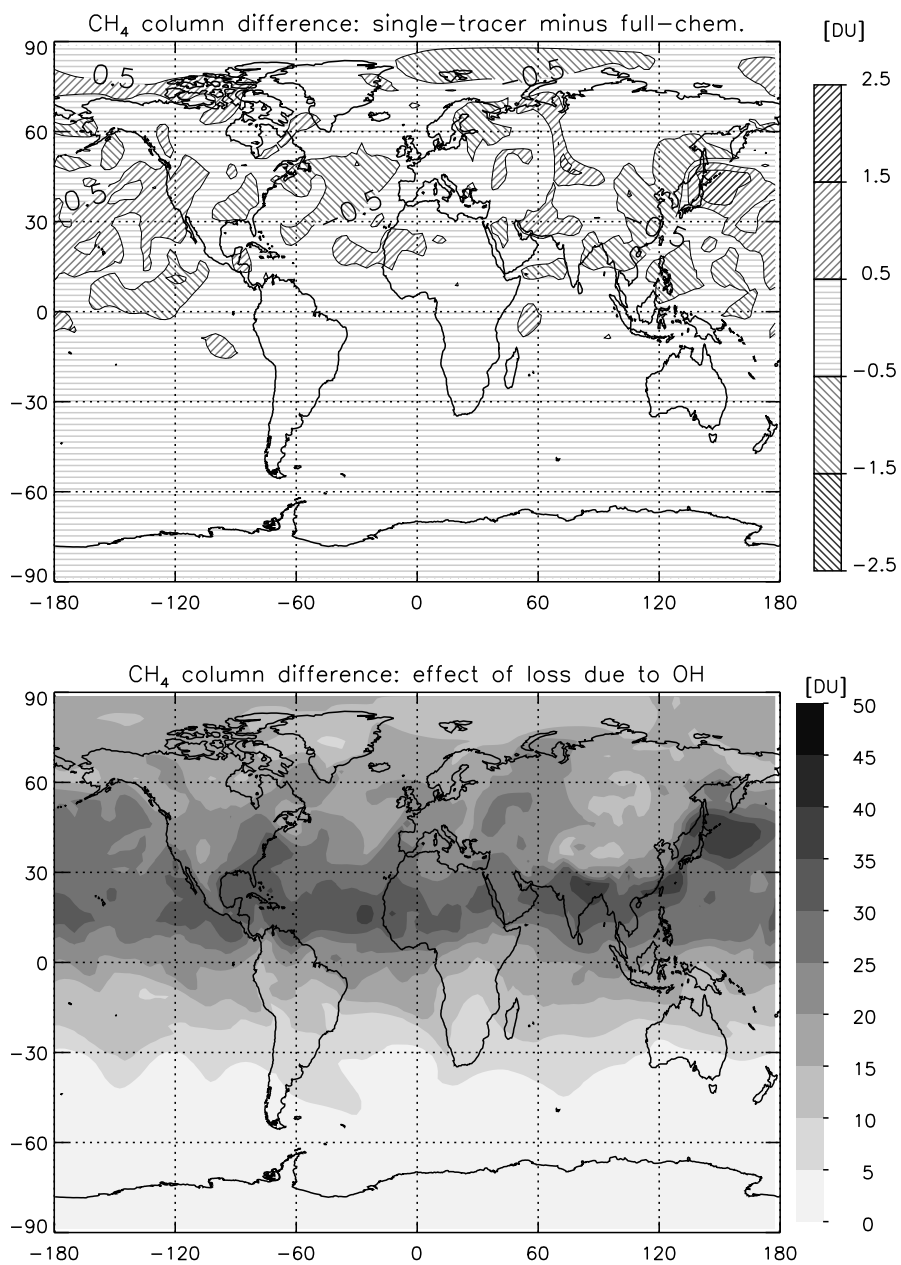


Figure 4.3: Top: difference between the instantaneous methane distribution from the single-tracer and full-chemistry versions at 00 UTC 31 July 2000, after one month of running on fine grid. Bottom: the same but now for a single-tracer version without CH_4 loss due to OH.

half that of GOME, and global coverage is reached in six days instead of three. The pixel size for SCIAMACHY is somewhat smaller than for GOME (30×240 km for the former versus 40×320 km for the latter). An advantage of the somewhat smaller pixel size of SCIAMACHY may be that a larger proportion of the pixels is cloud-free.

The ozone columns in the GOME level-2 files are replaced by methane columns taken from a forward run with TMSCIA, to which an amount of 10 DU is added. Moreover, an error estimate is added to these synthetic observations.

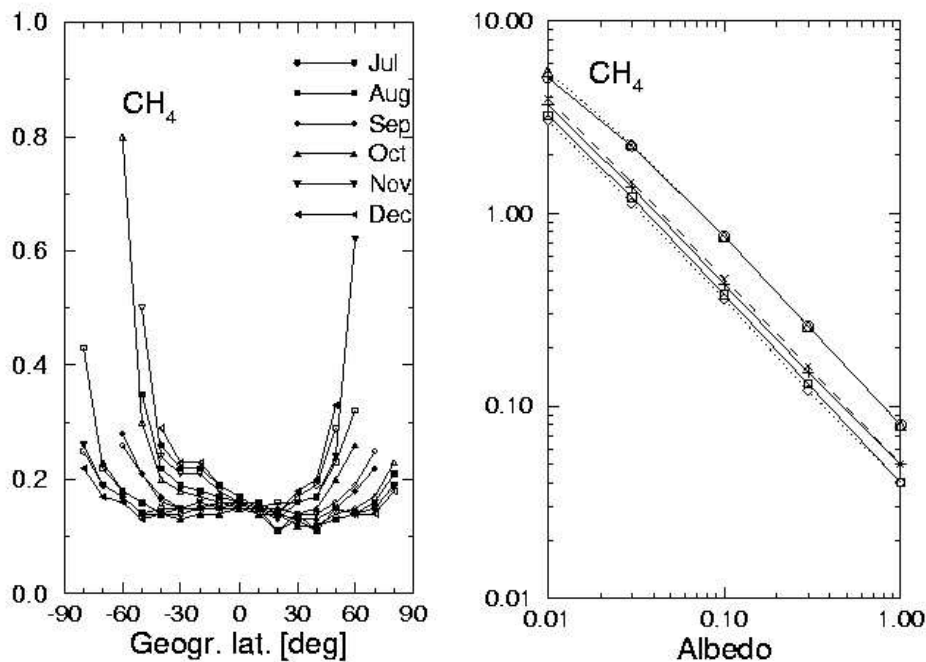


Figure 4.4: Sensitivity of SCIAMACHY CH_4 column observations in % (1σ): dependence on latitude (left) and albedo (right). In the left panel, the albedo is 0.2, and the line with filled squares is for July. In the right panel, the line with pluses is for 0° latitude. The figure is taken from Roemer et al. (1996).

The error in the retrieval of the methane column depends potentially on many factors. In this study, two such factors are taken into account: the influence of the solar zenith angle (or, alternatively, the latitude) and the influence of the albedo. Observation errors are specified according to figure 4.4 (see Roemer et al. 1996). It should be noted that these estimates are based on the instrument noise and resemble a best-case situation. Factors such as an imperfect knowledge of clouds will increase the uncertainty. To calculate the retrieval error, the albedo must be known. We have simply assumed an albedo of 0.05 over sea and 0.2 over land. In future studies this can be refined using global albedo maps on a monthly basis to take into account different soils and vegetations, and ice and snow.

As was mentioned before, the surface pressure has a dominating effect on the CH_4 column. For the present study this is no issue because the observations are taken from the model itself

and are thus consistent with the surface pressure in the model. For SCIAMACHY, the methane column observations will be combined with retrieved surface pressures into a mean mixing ratio, which is then assimilated in the model.

4.4.2 Results of the assimilation

The synthetic observations are assimilated in the model during one month. Since it is expected that clouds will be a serious problem for the retrieval, all pixels with a cloud cover of over 10% are skipped. The cloud cover is read from the GOME level-2 files (these values are based on the FRESKO algorithm, see Koelemeijer et al. 2001). All pixels with latitudes lower than -80° or higher than 80° are also skipped.

In the following simulations, the forecast error modelling (see equation 1.6 and further) is not performed. Instead, the forecast error is fixed at 3 DU. This value is chosen because it is of the same order as the observation error over land. As a result, information from both the model and the observations will be reflected in the analysis. The error in the superobservations is taken to be equal to the minimum of the errors of the pixels in a particular grid box. This corresponds to assuming that the observations within a model grid box are highly correlated. The observations are spread out in the model using a horizontal correlation function with a length scale of 500 km (see chapter 1).

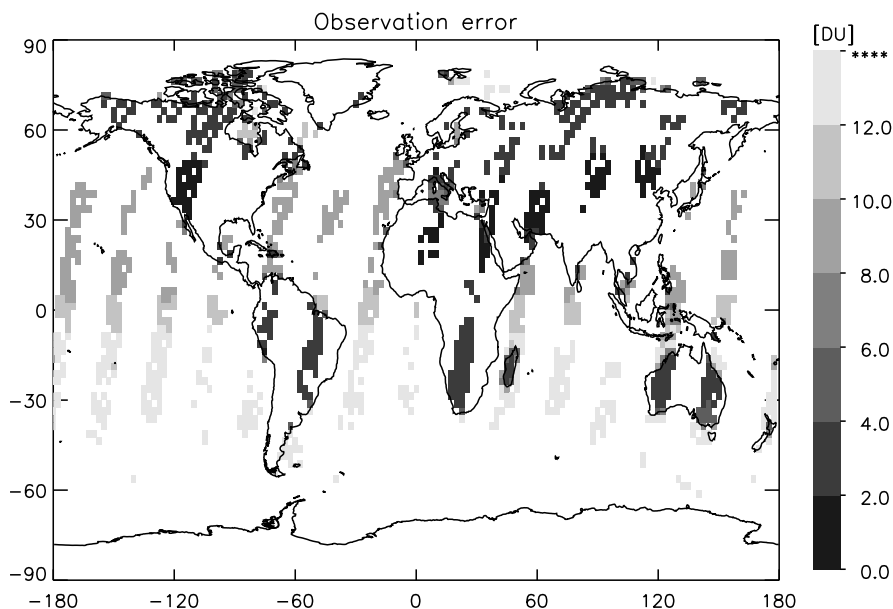


Figure 4.5: Estimated error in superobservations available after one day.

Figure 4.5 shows the error in the available superobservations after one day. Clearly, the demand

of a low cloud cover leads to large gaps in the experimental data. The difference in albedo over land and sea is also visible: over land the errors are about four times smaller. The best measurements in this month (July) are expected in the Northern Hemisphere since the solar zenith angle is smallest there. South of -40° no useful measurements are available.

Figure 4.6 shows the difference between the 'observed' methane column field (which is the result of the forward model run with 10 DU added everywhere) and the assimilated field. No adjustment to the observations corresponds to a value close to 10 DU in this figure, whereas full adjustment corresponds to 0 DU. In panel (a), after one day of assimilation, some features are clearly visible. First, the tracks of the satellite are characterized by smaller differences. This can be seen in particular between 120° W and 180° W, where the satellite has just passed. Over the Eurasian continent, horizontal advection has spread the information from the tracks. Second, the effect of the albedo, leading to higher observation errors over the sea, is recognizable (compare, for example, the continents Africa and South America with the Atlantic Ocean). Third, north of Canada, in particular, the assimilation has had a large impact. This is partly because the number of observations per unit area is larger. Partly it is also an artefact of the way the observations are treated. Near the Poles, the TM grid boxes cover a small area. As a result, the number of GOME pixels per grid box is relatively small. In contrast, the grid boxes near the Equator cover a large area, leading to more pixels per grid box. Since the observations within a grid box are considered to be strongly correlated and merged into one superobservation, the impact near the Equator will be smaller.

After one week of assimilation (panel b), the assimilation run is approaching the observations, particularly over the continents. South of -30° the difference between observations and assimilation is still large. Finally, after one month (panel c), the assimilation is within 1 DU from the observations. However, the information from the observations has still not propagated very much into the region south of -30° . Over the Himalaya and over Greenland the deviation is larger than 1 DU. There are also a few regions where the assimilation is *higher* than the observations (e.g., East China and North India). The cause of these particular features is unclear at the moment, and should be further investigated.

4.5 Conclusions

The TM3/TMSCIA model, which was described in this chapter, has proven to be a useful tool for performing global methane simulations. In the MEGGY project, the model was employed for estimating the sensitivity of methane columns to the underlying emissions. In a recent study by Dentener et al. (2002) the model was applied for assessing the inter-annual variability of methane emissions. In the present study, a CH_4 single-tracer version of TMSICA was developed and coupled to the data-assimilation system described in chapter 1. Synthetic satellite observations of CH_4 columns, with their expected (best-case) accuracy, were assimilated. Gaps in the data caused by the presence of clouds were also taken into account. The model column fields

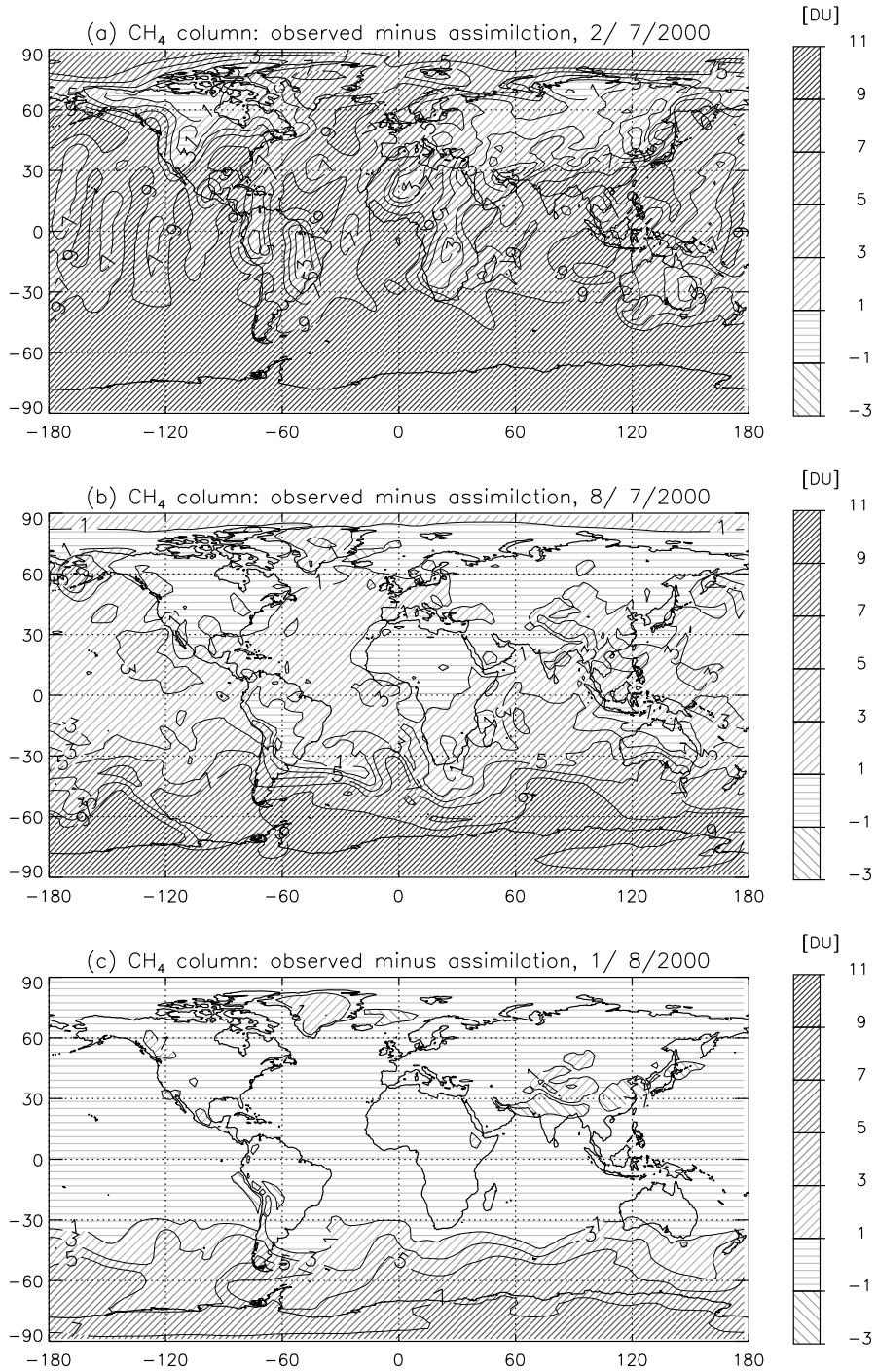


Figure 4.6: Observed (i.e. forward run plus 10 DU) minus assimilated methane column fields after (a) 1 day, (b) 1 week, and (c) 1 month of assimilation.

approach the synthetic observations globally on the timescale of a week, except for the southern part of the Southern Hemisphere, where no observations are present in the month July, which was considered.

Various aspects of the methane assimilation system are planned to be improved in the near future, in particular:

- More recent emission estimates (EDGAR 3)
As was outlined in this report, the characterization of methane sources is very important for simulating methane. New emission estimates from EDGAR should become available soon. These will be included in TMSICA.
- Extension to the stratosphere
The stratospheric variations in CH₄ have a significant influence on the total column. Thus, it is recommended that the model domain is extended above 10 hPa, following, for example, the ECMWF layer definition. The model simulations of total columns will certainly benefit from improved handling of stratospheric dynamics. In addition to the vertical domain extension, a simple description of stratospheric chemistry should be added, including the reactions by which CH₄ is lost.
- Nudging to surface observations
In order to maintain realistic background concentrations of CH₄ while running the model and assimilating satellite observations, it is useful to nudge the model to surface observations at remote locations, which are available from the NOAA-CMDL-FLASK program.

Outlook

The work performed in this project is part of on-going activities on the assimilation of GOME and SCIAMACHY measurements of the atmospheric composition in global chemistry-transport models. Phase 1 and 2 of the Sciamachy Data Assimilation project have led to the development of assimilation approaches for GOME total ozone, ozone profile information and methane, and a new assimilation-retrieval approach to NO₂. Combining observations with models of the atmospheric composition and circulation will extend the use of the satellite data data for scientific studies and model improvement. Monitoring of the atmosphere is important in relation to the possible recovery of the ozone layer (Montreal protocol) and the future development of greenhouse gas concentrations (Kyoto protocol).

Several new projects will benefit from the developments during Sciamachy Data Assimilation:

- ENVISAT validation campaign: The operational delivery of assimilated ozone fields and forecasts based on GOME data will be continued and extended to SCIAMACHY measurements as soon as these will be available. The assimilated fields will be used to support the SCIAMACHY validation campaign. In the ENVISAT AO project COMETH (Validation of CO and METHane SCIAMACHY data products) the SCIAMACHY data will be validated by comparison of assimilated global fields with MOPITT data and ground-based observations.
- Within the EU GOA project, a data base of five years of GOME assimilated ozone fields will be generated, and provided to the scientific community via the KNMI web site. Three dimensional ozone data set will be generated, based on the assimilation of ozone profiles.
- The ozone profile information from GOME and SCIAMACHY will be exploited, both by assimilating retrieved profiles and by directly assimilating radiances measured by the satellites (SRON-funded projects SASCIA and DROP).
- Future work on CH₄ (and also CO) modelling, assimilation and inverse modelling will be performed in the new EU project EVERGREEN (EnVisat for Environmental Regulation of GREENhouse gases; anticipated start date end 2002). This work will extend the methane modelling and assimilation developments described in this report.

In the years to come, new satellite instruments, such as OMI (Ozone Monitoring Instrument) and GOME-2, are planned for launch. The data assimilation infrastructure will be developed further and used for the interpretation of the observational data provided by SCIAMACHY and these future instruments.

Acknowledgements

We would like to thank several persons for their contributions to the work described in this report. Peter van Velthoven and Arjo Segers have provided the preprocessed meteorological fields from ECMWF. Pieter Valks has provided the near-real-time GOME ozone column data, and has created the internet interface to the operationally assimilated ozone fields and ozone forecasts. Dirk Olivié made significant improvements to the convection modelling in TMS-CIA. In the initial phase we have profited from the collaboration with the people involved in the MEGGY project, in particular Michiel Roemer, Peter Zandveld and Guus Velders. Anne Grete Straume is thanked for making available the error estimates for the methane column observations. The collaboration with the COMETH team (Ilse Aben, Anne Grete Straume, Hans Schrijver and Ahilleas Maurellis from SRON, and Maarten Krol from IMAU) on methane is gratefully acknowledged.

References

- Beswick, K. M., T. W. Simpson, D. Fowler, T. W. Choularton, M. W. Gallagher, K. J. Hargreaves, M. A. Sutton, and A. Kaye, 1998: Methane emissions on large scales. *Atmos. Env.*, **32(19)**, 3283–3291.
- Bovensmann, H., J. P. Burrows, M. Buchwitz, J. Frerick, S. Noel, V. V. Rozanov, K. V. Chance, and A. P. H. Goede, 1999: SCIAMACHY: Mission objectives and measurement modes. *J. Atmos. Sci.*, **56**, 127–150.
- Burrows, J. P., M. Weber, M. Buchwitz, V. Rozanov, A. Ladstätter-Weibenmayer, A. Richter, R. Debeek, R. Hoogen, K. Bramstedt, K.-U. Eichmann, M. Eisinger, and D. Perner, 1999: The Global Ozone Monitoring Experiment (GOME): Mission concept and first results. *J. Atmos. Sci.*, **56(2)**, 151–175.
- Dentener, F., M. van Weele, M. Krol, S. Houweling, and P. Van Velthoven, 2002: Trends and inter-annual variability of methane emissions derived from 1979–1993 global CTM simulations. *Atmos. Chem. Phys. Discuss.*, **2**, 249–287.
- Dlugokencky, E. J., B. P. Walter, K. A. Masarie, P. M. Lang, and E. S. Kasischke, 2001: Measurements of anomalous methane increase during 1998. *Geophys. Res. Lett.*, **28(3)**, 499–502.
- Eskes, H. J., 1999: Ozone satellite data analysis 2. USP-2 report 98-24, BCRS.
- Eskes, H. J., G. Y. El Serafy, and H. M. Kelder, 2001: Sciamachy data assimilation. USP-2 report 01-22, BCRS.
- Eskes, H. J., A. J. M. Piters, P. F. Levelt, M. A. F. Allaart, and H. M. Kelder, 1999: Variational assimilation of GOME total-column ozone satellite data in a 2D latitude-longitude tracer-transport model. *J. Atmos. Sci.*, **56**, 3560–3572.
- Eskes, H. J., P. F. J. Van Velthoven, and H. M. Kelder, 2002a: Ozone forecasting. To be submitted to *Atmos. Chem. Phys. Discuss.*
- Eskes, H. J., P. F. J. Van Velthoven, P. J. M. Valks, and H. M. Kelder, 2002b: Assimilation of GOME total ozone satellite observations in a three-dimensional tracer transport model. Submitted to *Q. J. R. Meteorol. Soc.*

- Fishman, J., C. E. Watson, J. C. Larsen, and J. A. Logan, 1990: Distribution of tropospheric ozone determined from satellite data. *J. Geophys. Res.*, **95**, 3599–3617.
- Fortuin, J. P. and H. M. Kelder, 1998: An ozone climatology based on ozonesonde and satellite measurements. *J. Geophys. Res.*, **103**, 31709–31734.
- Ganzeveld, L., J. Lelieveld, and G. J. Roelofs, 1997: A dry deposition parameterization for sulfur oxides in a chemistry and general circulation model. *J. Geophys. Res.*, **103**, 5679–5694.
- Guelle, W., Y. J. Balkanski, M. Schulz, F. Dulac, and P. Monfray, 1998: Wet deposition in a global size-dependent aerosol transport model, 1, Comparison of a 1 year Pb^{210} simulation with ground measurements. *J. Geophys. Res.*, **103**, 11429–11445.
- Gupta, M. L., R. J. Cicerone, and S. Elliot, 1998: Perturbation to global tropospheric oxidizing capacity due to latitudinal redistribution of surface sources of NO_x , CH_4 , and CO . *Geophys. Res. Lett.*, **21**, 3931–3934.
- Harries, J. E., H. E. Brindley, P. J. Sagoo, and R. J. Bantges, 2001: Increases in greenhouse forcing inferred from the outgoing longwave radiation spectra of the Earth in 1970 and 1997. *Nature*, **410**, 355–357.
- Houweling, S., 2000: *Global modeling of atmospheric methane sources and sinks*. PhD thesis, Utrecht University.
- Houweling, S., F. J. Dentener, and J. Lelieveld, 1998: The impact of non-methane hydrocarbon compounds on tropospheric photochemistry. *J. Geophys. Res.*, **103**, 10673–10696.
- Houweling, S., T. Kaminski, F. J. Dentener, J. Lelieveld, and M. Heimann, 1999: Inverse modelling of methane sources and sinks using the adjoint of a global transport model. *J. Geophys. Res.*, **104**, 26137–26160.
- IPCC, 2001: *Climate change 2001: The scientific basis*. Edited by J. T. Houghton et al., Cambridge University Press, UK and New York, NY, USA.
- Jeuken, A. B. M., H. J. Eskes, P. F. J. Van Velthoven, and H. M. Kelder, 1999: Assimilation of total ozone satellite measurements in a three-dimensional tracer transport model. *J. Geophys. Res.*, **104(D5)**, 5551–5563.
- Jeuken, A. B. M., P. F. J. Van Velthoven, G. Verver, H. M. Kelder, R. Ligtmans, M. Roemer, P. Builtjes, S. Houweling, L. Ganzeveld, and J. Lelieveld, 1997: Ozone satellite data modelling: Development of tools for setting up a system for assimilation of satellite derived ozone data. NRSP-2 report 96-10, BCRS.
- Karlsdóttir, S., 2000: *Model studies of methane in the atmosphere*. PhD thesis, University of Oslo.

- Khattatov, B. V., J.-F. Lamarque, L. V. Lyjak, R. Menard, P. F. Levelt, X. X. Tie, J. C. Gille, and G. P. Brasseur, 2000: Assimilation of satellite observations of long-lived chemical species in global chemistry-transport models. *J. Geophys. Res.*, **105**, 29135–29144.
- Koелеmeijer, R. B. A., P. Stammes, J. F. De Haan, and J. W. Hovenier, 2001: A fast method for retrieval of cloud parameters using oxygen A-band measurements from the Global Ozone Monitoring Experiment. *J. Geophys. Res.*, **106**, 3475–3490.
- Krol, M. and M. Van Weele, 1997: Implications of variation of photodissociation rates for global atmospheric chemistry. *Atmos. Env.*, **31**, 1257–1273.
- Landgraf, I. and P. J. Crutzen, 1998: An efficient method for online calculations of photolysis and heating rates. *J. Atmos. Sci.*, **55**, 863–878.
- Lelieveld, J. and F. J. Dentener, 2000: What controls tropospheric ozone? *J. Geophys. Res.*, **105**, 3531–3551.
- Levelt, P. F., M. A. F. Allaart, and H. M. Kelder, 1996: On the assimilation of total-ozone satellite data. *Ann. Geophysicae*, **14**, 1111–1115.
- Louis, J. F., 1979: A parametric model of vertical eddy fluxes in the atmosphere. *Boundary-Layer Meteorol.*, **17**, 187–202.
- Marland, G., T. A. Boden, and R. J. Andres, 2000: Global, regional, and national CO₂ emissions. Trends: A compendium of data on Global Change. Technical report, Carbon Dioxide Analysis Center, Oak Ridge National Laboratory, U.S. Department of Energy, Oak Ridge, Tenn., USA.
- McPeters, R. D., P. K. Bhartia, A. J. Krueger, J. R. Herman, C. G. Wellemeyer, C. J. Seftor, G. Jaross, O. Torres, L. Moy, G. Labow, W. Byerly, S. L. Taylor, T. Swissler, and R. P. Cebula, 1998: Earth Probe Total Ozone Mapping Spectrometer (TOMS) Data Products User's Guide. NASA Technical Publication 1998-206895, NASA Goddard Space Flight Center, Greenbelt, Maryland 20771.
- Olivier et al., J., 1996: Description of EDGAR version 2.0: A set of global emission inventories of greenhouse gases and ozone depleting substances for all anthropogenic and most natural sources on a per country basis on 1° × 1° grid. RIVM report 771060 002, RIVM, Bilthoven, The Netherlands.
- Prather, M. J., 1994: Lifetimes and eigenstates in atmospheric chemistry. *Geophys. Res. Let.*, **21(9)**, 801–804.
- Roemer, M., H. Schrijver, I. Aben, A. Goede, and S. Slijkhuis, 1996: Analysis of the potential of CO and CH₄ measurements by SCIAMACHY for the validation of tropospheric models. BCRS report NRSP-2, 96-36, BCRS.

- Roemer, M., P. Zandveld, P. Van Velthoven, M. Van Weele, and G. Velders, 2001a: Monitoring emissions of greenhouse gases using Sciamachy (MEGGY). Status report milestone 1 USP-2, 00-36, BCRS.
- Roemer, M., P. Zandveld, P. Van Velthoven, M. Van Weele, and G. Velders, 2001b: Monitoring emissions of greenhouse gases using Sciamachy (MEGGY). Status report milestone 2 USP-2, 01-42, BCRS.
- Russell, G. A. and J. A. Lerner, 1981: A new finite-differencing scheme for the tracer transport equation. *J. Appl. Meteorol.*, **20**, 1482–1498.
- Segers, A., P. Van Velthoven, B. Bregman, and M. Krol, 2002: On the computation of mass fluxes for Eulerian transport models from spectral meteorological fields. Submitted.
- Simmons, A. J., R. Mureau, and T. Petroliaigis, 1995: Error growth and estimates of predictability from the ECMWF forecasting. *Quart. J. Roy. Meteor. Soc.*, **121**, 1739–1771.
- Stoffelen, A., H. Eskes, and H. Kelder, 1999: The EU SODA project. Final report, KNMI, De Bilt, the Netherlands.
- Tiedtke, M., 1989: A comprehensive mass-flux scheme for cumulus parametrization in large-scale models. *Mon. Wea. Rev.*, **117**, 1778–1800.
- Štajner, I., L. P. Riishøjgaard, and R. B. Rood, 2000: The GEOS ozone data assimilation system: specification of error statistics. *Quart. J. Roy. Meteor. Soc.*, **127**, 1069–1094.
- Valks, P. J. M., A. J. M. Piters, J. C. Lambert, C. Zehner, and H. Kelder, 2002: A fast delivery system for the retrieval of near-real time ozone columns from GOME data. Accepted for publication in *Int. J. Remote Sensing*.
- Van Aardenne, J. A., F. J. Dentener, C. G. M. Klein Goldewijk, J. Lelieveld, and J. G. J. Olivier, 2001: A high resolution data set of historical anthropogenic trace gas emissions for the period 1890–1990. *Global Biogeochemical Cycles*, **15**, 909–928.
- Van der A, R. J., H. J. Eskes, J. Van Geffen, R. F. Van Oss, A. J. M. Piters, P. J. M. Valks, and C. Zehner, 2000: GOME Fast delivery and value-Added Products (GOFAP). In *Proceedings of the ESA ERS - ENVISAT symposium*, pages 1–1. Gothenburg, Sweden, 16-20 October.
- Van Velthoven, P. F. J. and H. M. Kelder, 1996: Estimates of stratosphere–troposphere exchange: Sensitivity to model formulation and horizontal resolution. *J. Geophys. Res.*, **101**, 1429–1434.
- Warneck, P., 1988: *Chemistry of the natural atmosphere*, volume 41 of *International Geophysics Series*. Academic Press Inc., London, England. 757 pp.